ANNUAL REVIEWS

Annual Review of Control, Robotics, and Autonomous Systems

Control of Low-Inertia Power Systems

Florian Dörfler[1] and Dominic Groß[2]

[1]Automatic Control Laboratory, ETH Zurich, Zurich, Switzerland; email: dorfler@ethz.ch

[2]Department of Electrical and Computer Engineering, University of Wisconsin–Madison, Madison, Wisconsin, USA; email: dominic.gross@wisc.edu

Annu. Rev. Control Robot. Auton. Syst. 2023. 6:415–45

First published as a Review in Advance on October 6, 2022

The *Annual Review of Control, Robotics, and Autonomous Systems* is online at control.annualreviews.org

https://doi.org/10.1146/annurev-control-052622-032657

Keywords

power systems control, power electronics control, low-inertia systems, grid-forming control, dynamic virtual power plant

Abstract

Electric power systems are undergoing an unprecedented transition from fossil fuel–based power plants to low-inertia systems that rely predominantly on power electronics and renewable energy resources. This article reviews the resulting control challenges and modeling fallacies, at both the device and system level, and focuses on novel aspects or classical concepts that need to be revised in light of the transition to low-inertia systems. To this end, we survey the literature on modeling of low-inertia systems, review research on the control of grid-connected power converters, and discuss the frequency dynamics of low-inertia systems. Moreover, we discuss system-level services from a control perspective. Overall, we conclude that the system-theoretic mindset is essential to bridge different research communities and understand the complex interactions of power electronics, electric machines, and their controls in large-scale low-inertia power systems.

1. INTRODUCTION

The future electric power system is envisioned to be both sustainable and highly resilient. An ever-increasing share of conventional fossil fuel–based power plants is being replaced by renewable energy resources. This transition to a sustainable system involves the major challenge of replacing bulk generation interfaced with synchronous machines with distributed generation interfaced primarily with power electronics. Unlike past evolutions of the electric power system, these unprecedented changes affect its very core, namely, the power generation and conversion technology: from conventional rotational power generation based on synchronous machines toward converter-interfaced generation (CIG) and conversion, as in the case of renewable energy sources, battery storage, or high-voltage DC (HVDC) links interconnecting different synchronous areas. This transition poses major challenges to the operation, control, stability, and resilience of the power system due to (*a*) the loss of rotational kinetic energy in synchronous machines, whose inertia acts a safeguard against disturbances; (*b*) the loss of the stable and robust nonlinear synchronization mechanism that is physically inherent to rotational generation; and (*c*) the loss of robust frequency and voltage control as well as stabilizing ancillary services provided by synchronous machines—all of which are paired with the variability and intermittency of renewable generation.

In this review, we refer to recent surveys, tutorials, and magazine articles that have illustrated the various challenges of future so-called low-inertia power systems from the perspective of power systems, power electronics, and controls (1–13). A universal conclusion is that the modeling, stability analysis, simulation, and control of low-inertia systems need to be revisited, and many canonical concepts must be questioned. Doing so will help bring about a confluence of the (thus far mostly disjoint) power systems and power electronics communities, whose interactions can be facilitated by systems and control theory acting as the common lingua franca.

Here, we take the systems and control perspective and review the modeling fallacies and control challenges of low-inertia power systems as well as some first solutions that have been put forward. We cover both device-level and system-level aspects. We do not aim to be comprehensive in our scope, focusing predominantly on either novel aspects or traditional concepts that need to be revised in low-inertia systems. Inevitably, this article is colored and biased by our own research interests and experiences and does not present all viewpoints on or facets of the topic of low-inertia power systems.

The remainder of the article is organized as follows. Section 2 reviews salient elements of low-inertia systems and their models. Section 3 discusses the control of grid-connected converters. Section 4 discusses the frequency dynamics of low-inertia systems. Finally, Section 5 discusses the system-level services and controls aspects.

2. SALIENT ELEMENTS OF LOW-INERTIA SYSTEMS AND THEIR MODELS

In this section, we briefly recap the modeling of AC power systems with a particular focus on salient elements of future low-inertia systems, i.e., time-domain models of the network circuitry and device-level models of synchronous machines and power converters. For further details, we refer readers to relevant textbooks covering the modeling of power systems and grid-connected power converters (14–16).

2.1. Three-Phase AC Power System

Broadly speaking, a power system consists of generation, load, and the circuitry (i.e., the power network) interconnecting them. We begin with the last and direct readers to References 17–19 and references therein for network-theoretic or port-Hamiltonian modeling perspectives.

2.1.1. Power network model.

We model the network as a graph with nodes (or buses) $\mathcal{V}$, edges (or lines or branches) $\mathcal{E} \subset \mathcal{V} \times \mathcal{V}$, and an oriented node–edge incidence matrix $B \in \mathbb{R}^{|\mathcal{V}| \times |\mathcal{E}|}$:

$$B_{ie} = \begin{cases} +1, & \text{if the edge } e \text{ is } (i, j) \text{ for some } j, \\ -1, & \text{if the edge } e \text{ is } (j, i) \text{ for some } j, \\ 0, & \text{otherwise.} \end{cases}$$

For every bus $i \in \mathcal{V}$, we define a potential (or nodal voltage) $\mathbf{v}_i \in \mathbb{R}^3$ and an exogenous current injection $\mathbf{I}_i \in \mathbb{R}^3$. Likewise, for every branch $e \in \mathcal{E}$ we define an oriented current flow $\mathbf{i}_e \in \mathbb{R}^3$ and an oriented voltage drop $\mathbf{u}_e \in \mathbb{R}^3$. All currents and voltages are three-phase signals with components labeled *abc*, e.g., $\mathbf{v}_i = [\, v_{i,a} \;\; v_{i,b} \;\; v_{i,c} \,]^\top$. We discuss the signal space in Section 2.1.2. Kirchhoff's voltage and current laws relate these signals as

$$\mathbf{I} = \mathbf{B}\mathbf{i} \qquad \text{and} \qquad \mathbf{u} = \mathbf{B}^\top \mathbf{v}, \tag{1}$$

where we defined the shorthands $\mathbf{B} := (B \otimes \mathcal{I}_3)$, $\mathbf{I} := (\mathbf{I}_1, \ldots, \mathbf{I}_{|\mathcal{V}|})$, $\mathbf{v} := (\mathbf{v}_1, \ldots, \mathbf{v}_{|\mathcal{V}|})$, $\mathbf{u} := (\mathbf{u}_1, \ldots, \mathbf{u}_{|\mathcal{E}|})$, and $\mathbf{i} := (\mathbf{i}_1, \ldots, \mathbf{i}_{|\mathcal{E}|})$, where $\mathcal{I}_3$ denotes the 3×3 identity matrix.

We further complement Kirchhoff's laws through constitutive relations (such as Ohm's law) relating $\mathbf{i}_e$ and $\mathbf{u}_e$ for any branch $e \in \mathcal{E}$. The three typical constitutive relations are as follows:

- Resistive: $\mathbf{u}_e = r_e \mathbf{i}_e$, where $r_e > 0$ is a resistance.
- Inductive: $l_e \frac{\mathrm{d}}{\mathrm{d}t} \mathbf{i}_e = \mathbf{u}_e$, where $l_e > 0$ is an inductance.
- Capacitive: $c_e \frac{\mathrm{d}}{\mathrm{d}t} \mathbf{u}_e = \mathbf{i}_e$, where $c_e > 0$ is a capacitance.

Observe that here we have implicitly assumed that the circuitry is symmetric, i.e., that r_e, l_e, and c_e are scalar parameters rather than general 3×3 matrices accounting for nonuniformities and interactions among phases (20, 21). This assumption is valid for high-voltage transmission systems commonly considered in the literature on low-inertia systems (15, 22). Finally, power system specifications are often given in units of power. Loosely speaking, power is the product of current and voltage. However, there are many coexisting definitions of power, especially for reactive power (23, 24). It makes sense to define power in particular coordinates attached to a three-phase system, which are introduced in Section 2.1.2.

2.1.2. Three-phase signals: specifications and coordinate frames.

Consider a three-phase circuit signal $\mathbf{x}_{abc} = [\, x_a \;\; x_b \;\; x_c \,]^\top \in \mathbb{R}^3$, e.g., any nodal or branch voltage/current. Three-phase signals in power transmission systems are not arbitrary; due to three-wire transmission, three-phase generation and conversion, and control, they are

- periodic with zero average, $\frac{1}{T} \int_0^T x_i(\tau)\, \mathrm{d}\tau = 0$ for some $T > 0$ and for all $i \in \{a, b, c\}$;
- balanced, $\mathbf{x}_{abc} = A(t) \begin{bmatrix} \sin(\delta(t)) \\ \sin(\delta(t) - \frac{2\pi}{3}) \\ \sin(\delta(t) + \frac{2\pi}{3}) \end{bmatrix}$ for some time-varying angle $\delta(t)$ and non-negative amplitude $A(t)$, so that $x_a(t) + x_b(t) + x_c(t) = 0$ for all $t \geq 0$; and
- synchronous (in steady state) with constant frequency ω, $\mathbf{x}_{abc} = A \begin{bmatrix} \sin(\delta + \omega t) \\ \sin(\delta + \omega t - \frac{2\pi}{3}) \\ \sin(\delta + \omega t + \frac{2\pi}{3}) \end{bmatrix}$ for some constant amplitude A and angle δ.

For the problems considered in this article, it is fair to assume that all signals are periodic and balanced, and the role of analysis and control design is to certify stability of synchronous solutions, where all signals in the circuit have a common synchronous frequency ω (14, 22).

COORDINATE FRAMES FOR THREE-PHASE SIGNALS

Consider a periodic and balanced three-phase signal

$$\mathbf{x}_{abc} = \begin{bmatrix} x_a \\ x_b \\ x_c \end{bmatrix} = A \begin{bmatrix} \sin(\delta) \\ \sin(\delta - \frac{2\pi}{3}) \\ \sin(\delta + \frac{2\pi}{3}) \end{bmatrix},$$

where we omitted the dependence of $\mathbf{x}_{abc}$, A, and δ on time. Balancedness implies that $\mathbf{x}_{abc}$ is orthogonal to $[\,1\ 1\ 1\,]$. Consider the orthonormal Clarke transform $\mathbf{T}_{\alpha\beta 0}$: $\mathbf{x}_{abc} \to \mathbf{x}_{\alpha\beta 0}$ removing the balanced subspace:

$$\mathbf{T}_{\alpha\beta 0} = \sqrt{\tfrac{2}{3}} \left[\begin{array}{ccc} 1 & -\frac{1}{2} & -\frac{1}{2} \\ 0 & \frac{\sqrt{3}}{2} & -\frac{\sqrt{3}}{2} \\ \hline \frac{1}{\sqrt{2}} & \frac{1}{\sqrt{2}} & \frac{1}{\sqrt{2}} \end{array}\right].$$

The resulting coordinate frame is denoted by $\alpha\beta 0$, and the signal $\mathbf{x}_{\alpha\beta 0} = \mathbf{T}_{\alpha\beta 0}\mathbf{x}_{abc}$ satisfies

$$\mathbf{x}_{\alpha\beta 0} = \left[\begin{array}{c} x_\alpha \\ x_\beta \\ \hline x_0 \end{array}\right] = \sqrt{\tfrac{3}{2}} A \left[\begin{array}{c} \sin(\delta) \\ -\cos(\delta) \\ \hline 0 \end{array}\right].$$

Next, consider the orthonormal Park transform $\mathbf{T}_{dq0}(\theta)$: $\mathbf{x}_{\alpha\beta 0} \to \mathbf{x}_{dq0}$ into a rotating frame with angle θ:

$$\mathbf{T}_{dq0}(\theta) = \sqrt{\tfrac{2}{3}} \left[\begin{array}{ccc} \cos(\theta) & -\sin(\theta) & 0 \\ \sin(\theta) & \cos(\theta) & 0 \\ \hline 0 & 0 & 1 \end{array}\right].$$

The resulting coordinate frame is denoted by $dq0$, and the signal $\mathbf{x}_{dq0} = \mathbf{T}_{dq0}(\theta)\mathbf{x}_{\alpha\beta 0}$ satisfies

$$\mathbf{x}_{dq0} = \left[\begin{array}{c} x_d \\ x_q \\ \hline x_0 \end{array}\right] = \sqrt{\tfrac{3}{2}} A \left[\begin{array}{c} \sin(\delta+\theta) \\ -\cos(\delta+\theta) \\ \hline 0 \end{array}\right] \overset{\theta=-\delta}{=} \sqrt{\tfrac{3}{2}} A \left[\begin{array}{c} 0 \\ -1 \\ \hline 0 \end{array}\right].$$

The component x_0 is normally discarded in a balanced system, and the remaining $\mathbf{x}_{dq}$ coordinates are denoted by a phasor $\sqrt{\frac{3}{2}}A\left[\begin{smallmatrix} \sin(\delta+\theta) \\ -\cos(\delta+\theta) \end{smallmatrix}\right]$ or, in complex coordinates, $\sqrt{\frac{3}{2}}Ae^{\mathrm{j}(\delta-\theta)}$. The overall transform is

$$\mathbf{T}_{dq0} \cdot \mathbf{T}_{\alpha\beta 0} = \sqrt{\tfrac{2}{3}} \left[\begin{array}{ccc} \cos(\theta) & \cos\left(\theta + \frac{2\pi}{3}\right) & \cos\left(\theta - \frac{2\pi}{3}\right) \\ \sin(\theta) & \sin\left(\theta + \frac{2\pi}{3}\right) & \sin\left(\theta - \frac{2\pi}{3}\right) \\ \hline \frac{\sqrt{2}}{2} & \frac{\sqrt{2}}{2} & \frac{\sqrt{2}}{2} \end{array}\right].$$

Many coordinate frames and representations have been introduced to study three-phase signals (see the sidebar titled Coordinate Frames for Three-Phase Signals and, e.g., Reference 25). Throughout this article, we work in a $dq0$ frame induced by the orthonormal (i.e., power-invariant) Park transform attached to the nominal AC network frequency ω_0 (e.g., $\omega_0 = 2\pi \cdot 50$ Hz or $\omega_0 = 2\pi \cdot 60$ Hz), we drop the zero component, and we generally omit the subscripts abc, $\alpha\beta$, dq, and so on. Readers may convince themselves that in such a coordinate frame the constitutive relations for inductor and resistor change to

$$l_e \tfrac{\mathrm{d}}{\mathrm{d}t}\mathbf{i}_e = -\mathbf{J}\omega_0 l_e \mathbf{i}_e + \mathbf{u}_e \qquad \text{and} \qquad c_e \tfrac{\mathrm{d}}{\mathrm{d}t}\mathbf{u}_e = -\mathbf{J}\omega_0 c_e \mathbf{u}_e + \mathbf{i}_e,$$

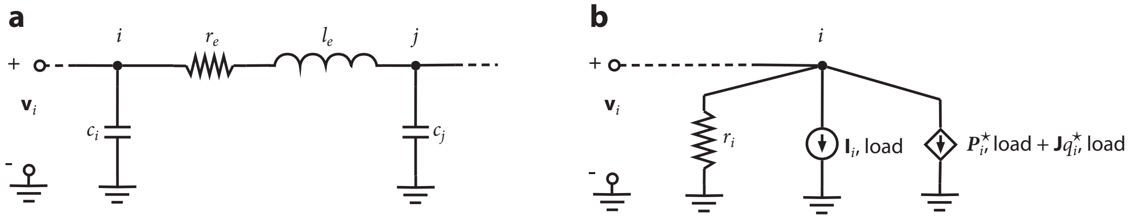

Figure 1

(*a*) Π model of a power line and (*b*) schematic illustration of a ZIP load (where Z, I, and P stand for the impedance, current, and power contributions, respectively).

where the 90° rotation matrix $\mathbf{J} = \left[\begin{smallmatrix} 0 & -1 \\ 1 & 0 \end{smallmatrix}\right]$ is the analogue of the imaginary unit $\mathrm{j} = \sqrt{-1}$. This analogy is deliberate since $\mathbf{J}^2 = -\mathcal{I}$, $\mathbf{J}^\top = -\mathbf{J}$, and the terms $\mathbf{J}\omega_0 l_e$ and $\mathbf{J}\omega_0 c_e$ recover the familiar complex-valued formulations of inductive and capacitive impedances.

Among the many definitions of active and reactive power, we use instantaneous power (23, 25). Namely, for a current $\mathbf{i}$ and voltage $\mathbf{v}$ at the same bus, active power is defined as

$$p = \mathbf{i}^\top \mathbf{v}, \tag{2.}$$

i.e., an inner product, and reactive power is defined by the cross product written as

$$q = \mathbf{i}^\top \mathbf{J}\mathbf{v}, \tag{3.}$$

which is equal to the positive sequence powers of a standard three-phase phasor model.

2.1.3. Line and load dynamics.

We specify the exogenous current injection at node i as

$$\mathbf{I}_i = \mathbf{I}_{i,\mathrm{g}} - \mathbf{I}_{i,\mathrm{load}} - \mathbf{I}_{i,\mathrm{charge}}, \tag{4.}$$

accounting for the dynamic contribution of generation, loads, and line charging. Generation is specified in Section 2.2; here, we focus on loads and line charging and the constitutive relations.

Power system lines are typically specified by the Π model (see **Figure 1**). A series of resistive and inductive elements models the inductance and losses of line $e \in \mathcal{E}$ as

$$l_e \tfrac{\mathrm{d}}{\mathrm{d}t}\mathbf{i}_e = -(r_e \mathcal{I} + \mathbf{J}\omega_0 l_e)\mathbf{i}_e + \mathbf{u}_e. \tag{5.}$$

Lines range from dominantly inductive (in high-voltage transmission) to equally inductive and resistive (in low-voltage distribution). Furthermore, the charging effect of the line is modeled by a capacitive connection to the ground on either end of the line, i.e.,

$$c_i \tfrac{\mathrm{d}}{\mathrm{d}t}\mathbf{v}_i = \mathbf{I}_{i,\mathrm{charge}}. \tag{6.}$$

We do not discuss the detailed modeling of loads; for more information on this modeling, we direct readers to References 14 and 15. For the considered problems, it is typically sufficient to model loads on an aggregate level as mere shunt resistances r_i (sometimes also inductances) or as sinks drawing either constant current $\mathbf{I}^\star_{i,\mathrm{load}}$ or constant active and reactive power—i.e., $p_{i,\mathrm{load}} = \mathbf{I}^\top_{i,\mathrm{load}}\mathbf{v}_i$ and $q_{i,\mathrm{load}} = \mathbf{I}^\top_{i,\mathrm{load}}\mathbf{J}\mathbf{v}_i$:

$$\mathbf{I}_{i,\mathrm{load}} = \frac{1}{r_i}\mathbf{v}_i + \mathbf{I}^\star_{i,\mathrm{load}} + \tfrac{1}{\|\mathbf{v}_i\|^2}\left(p_{i,\mathrm{load}}\mathcal{I} + q_{i,\mathrm{load}}\mathbf{J}\right)\mathbf{v}_i \tag{7.}$$

(see **Figure 1**). Such loads are colloquially termed ZIP loads, where Z, I, and P stand for the impedance, current, and power contributions, respectively, and many variations thereof have been proposed.

The network model given by Equations 1–7 in dq coordinates reads compactly as

$$\begin{bmatrix} \mathbf{L}\frac{\mathrm{d}}{\mathrm{d}t}\mathbf{i} \\ \mathbf{C}\frac{\mathrm{d}}{\mathrm{d}t}\mathbf{v} \end{bmatrix} = \begin{bmatrix} -\mathbf{Z} & \mathbf{B}^\top \\ -\mathbf{B} & -\mathbf{G}(\mathbf{v}) \end{bmatrix} \begin{bmatrix} \mathbf{i} \\ \mathbf{v} \end{bmatrix} + \begin{bmatrix} 0 \\ \mathbf{I}_\mathrm{g} - \mathbf{I}^\star_\mathrm{load} \end{bmatrix}, \tag{8}$$

where we eliminated the voltage drops $\mathbf{u}_e$; $\mathbf{i}$ and $\mathbf{v}$ are vectors collecting $\mathbf{i}_e$ and $\mathbf{v}_i$, respectively; $\mathbf{I}_\mathrm{g}$ and $\mathbf{I}^\star_\mathrm{load}$ are vectors collecting all generation inputs and constant current loads, respectively; and we lumped the circuit and load parameters into the diagonal matrices $\mathbf{L} = \mathrm{diag}(l_e\mathcal{I})$, $\mathbf{C} = \mathrm{diag}(c_i\mathcal{I})$, $\mathbf{Z} = \mathrm{diag}(r_e\mathcal{I} + \mathbf{J}\omega_0 l_e)$, and $\mathbf{G}(\mathbf{v}) = \mathrm{diag}(\frac{1}{r_i}\mathcal{I} + \frac{1}{\|\mathbf{v}_i\|^2}(p_{i,\mathrm{load}}\mathcal{I} + q_{i,\mathrm{load}}\mathbf{J}))$.

The network model in Equation 8 is directly amenable to a graph-theoretic (18) or passivity (19) analysis. For a glimpse into the latter, consider the network power balance

$$\begin{aligned}
\underbrace{\tfrac{\mathrm{d}}{\mathrm{d}t}\left(\tfrac{1}{2}\mathbf{i}^\top\mathbf{L}\mathbf{i} + \tfrac{1}{2}\mathbf{v}^\top\mathbf{C}\mathbf{v}\right)}_{\frac{\mathrm{d}}{\mathrm{d}t}\text{ stored energy}} = {} & \underbrace{\begin{bmatrix} \mathbf{i} \\ \mathbf{v} \end{bmatrix}^\top \begin{bmatrix} -\mathrm{diag}\,(\mathbf{J}\omega_0 l_e) & \mathbf{B}^\top \\ -\mathbf{B} & -\mathrm{diag}\left(\frac{1}{\|\mathbf{v}_i\|^2} q_{i,\mathrm{load}}\,\mathbf{J}\right) \end{bmatrix} \begin{bmatrix} \mathbf{i} \\ \mathbf{v} \end{bmatrix}}_{=\,0\text{ reactive/circulating power}} \\
& \underbrace{-\sum\nolimits_{i\in\mathcal{V}} p_{i,\mathrm{load}} - \mathbf{v}^\top\mathbf{I}^\star_\mathrm{load} - \mathbf{v}^\top\mathrm{diag}\left(\tfrac{1}{r_i}\right)\mathbf{v}}_{\text{active power consumed by loads}} \\
& -\underbrace{\mathbf{i}^\top\mathrm{diag}\,(r_e\mathcal{I})\,\mathbf{i}}_{\text{line losses}} + \underbrace{\mathbf{v}^\top\mathbf{I}_\mathrm{g}}_{\substack{\text{power supplied}\\ \text{by generation}}}
\end{aligned}$$

transparently depicting the net-zero contributions from reactive elements, power dissipated by loads and lines, and power supplied by generation sources modeled as current sources $\mathbf{I}_{i,\mathrm{g}}$. Section 2.2 further specifies the modeling of the latter.

2.2. Device-Level Models: Synchronous Machines and Power Converters

Our subsequent discussion of device-level models focuses on synchronous machines and grid-connected power converters, their similarities, and their differences.

2.2.1. Synchronous machine.

A synchronous machine converts mechanical to electrical energy by means of a rotating magnetic field that induces torques on the rotor of the machine and currents on the stator of the machine. We direct readers to Reference 22 for a comprehensive discussion of modeling and to Reference 19 for an intriguing port-Hamiltonian perspective.

Here, we consider a standard synchronous machine model (depicted in **Figure 2**) and make the following assumptions: The rotor is nonsalient and features a single-pole pair, DC excitation, and no damper windings. The rotor has a rotational inertia M and damping D and is driven by the

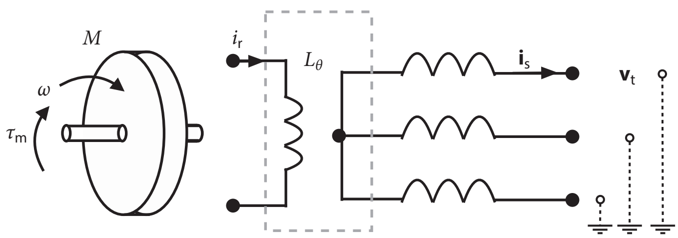

Figure 2

A synchronous machine. The rotor with speed ω and angle θ is driven by the mechanical torque. Mechanical power is converted to electrical power through the rotor, stator, and mutual inductances modeled by L_θ.

(controllable) torque τ_{m} from the turbine/governor; its state variables are the angle θ and angular velocity ω. The energy stored in the rotating magnetic field is

$$W = \tfrac{1}{2}\begin{bmatrix}\mathbf{i}_{\mathrm{s}} \\ i_{\mathrm{r}}\end{bmatrix}^{\top} \mathbf{L}_{\theta} \begin{bmatrix}\mathbf{i}_{\mathrm{s}} \\ i_{\mathrm{r}}\end{bmatrix},$$

where $\mathbf{i}_{\mathrm{s}}$ and i_{r} are the three-phase (in *abc*) stator and DC rotor flux currents, respectively, and

$$\mathbf{L}_{\theta} = \begin{bmatrix} L_{\mathrm{s}} & 0 & 0 & L_{\mathrm{m}}\cos(\theta) \\ 0 & L_{\mathrm{s}} & 0 & L_{\mathrm{m}}\cos(\theta - \frac{2\pi}{3}) \\ 0 & 0 & L_{\mathrm{s}} & L_{\mathrm{m}}\cos(\theta + \frac{2\pi}{3}) \\ L_{\mathrm{m}}\cos(\theta) & L_{\mathrm{m}}\cos(\theta - \frac{2\pi}{3}) & L_{\mathrm{m}}\cos(\theta + \frac{2\pi}{3}) & L_{\mathrm{r}} \end{bmatrix}$$

is the inductance matrix with the stator, rotor, and mutual inductances L_{s}, L_{r}, and L_{m}, respectively. The mechanical dynamics are then (in a frame rotating with ω_0) described by

$$\frac{\mathrm{d}\theta}{\mathrm{d}t} = \omega - \omega_0 \quad \text{and} \quad M\frac{\mathrm{d}\omega}{\mathrm{d}t} = -D\omega + \tau_{\mathrm{m}} - \tau_{\mathrm{e}},$$

where $\tau_{\mathrm{e}} = \frac{\partial W}{\partial \theta}$ is the air gap torque. The damping D due to mechanical and electrical losses is negligible, and often D models the equivalent load damping and damping due to damper windings. The flux linkage equations are then (in *abc* coordinates)

$$\frac{\mathrm{d}}{\mathrm{d}t}\left(\mathbf{L}_{\theta}\begin{bmatrix}\mathbf{i}_{\mathrm{s}} \\ i_{\mathrm{r}}\end{bmatrix}\right) = \begin{bmatrix} -R_{\mathrm{s}}\mathcal{I} & \\ & -R_{\mathrm{r}}\end{bmatrix}\begin{bmatrix}\mathbf{i}_{\mathrm{s}} \\ i_{\mathrm{r}}\end{bmatrix} + \begin{bmatrix}\mathbf{v}_{\mathrm{t}} \\ u_{\mathrm{r}}\end{bmatrix},$$

where R_{s} and R_{r} are resistive losses in the stator and rotor coils, respectively; u_{r} is the controllable DC rotor excitation voltage; and $\mathbf{v}_{\mathrm{t}}$ is the three-phase terminal voltage.

When formulating these equations in a *dq* frame rotating with ω_0 and assuming tight control via u_{r} of i_{r} to a reference input (also denoted by i_{r} for simplicity), we arrive at the air gap torque $\tau_{\mathrm{e}} = L_{\mathrm{m}} i_{\mathrm{r}} \begin{bmatrix} -\sin\theta \\ \cos\theta \end{bmatrix}^{\top} \mathbf{i}_{\mathrm{s}}$, the induced voltage $\mathbf{v}_{\mathrm{ind}} = L_{\mathrm{m}} i_{\mathrm{r}} \begin{bmatrix} -\sin\theta \\ \cos\theta \end{bmatrix} \omega$, and thus

$$\begin{aligned} \frac{\mathrm{d}\theta}{\mathrm{d}t} &= \omega - \omega_0, \\ M\frac{\mathrm{d}\omega}{\mathrm{d}t} &= -D\omega + \tau_{\mathrm{m}} - L_{\mathrm{m}} i_{\mathrm{r}} \begin{bmatrix} -\sin\theta \\ \cos\theta \end{bmatrix}^{\top} \mathbf{i}_{\mathrm{s}}, \\ L_{\mathrm{s}}\frac{\mathrm{d}\mathbf{i}_{\mathrm{s}}}{\mathrm{d}t} &= -(R_{\mathrm{s}}\mathcal{I} + \mathbf{J}\omega_0 L_{\mathrm{s}})\mathbf{i}_{\mathrm{s}} + L_{\mathrm{m}} i_{\mathrm{r}} \begin{bmatrix} -\sin\theta \\ \cos\theta \end{bmatrix} \omega - \mathbf{v}_t. \end{aligned} \tag{9}$$

The assumptions underlying the model in Equation 9 can be lifted (26), but this model suffices for our discussion. Depending on whether the synchronous machine supplies or absorbs power, it is referred to as a synchronous generator (SG) or synchronous motor, respectively. We investigate the former here.

For an SG, we note that one normally models the (relatively slow) mechanical actuation via the turbine/governor system on τ_{m} through a series of linear filters [typically low pass but sometimes also featuring unstable zeros (14)], giving rise to a delay and sometimes inverse response dynamics. The stability analysis of multimachine power systems typically leverages reduced-order linearized synchronous machine and turbine models (see the sidebar titled Reduced-Order Synchronous Generator and Turbine Models).

REDUCED-ORDER SYNCHRONOUS GENERATOR AND TURBINE MODELS

Low-order approximations of the SG dynamics in Equation 9 are commonly used for stability analysis or for gaining qualitative insights into the dynamics. The dynamics of an SG with excitation are commonly represented by the classical one-axis generator model with exciter (also known as the third-order model), given by (15, 22, 27, 28)

$$\frac{\mathrm{d}\theta}{\mathrm{d}t} = \omega - \omega_0, \qquad \text{S1a.}$$

$$\frac{2H}{\omega_0}\frac{\mathrm{d}\omega}{\mathrm{d}t} = -D\omega + p_\mathrm{m} - p_\mathrm{g}, \qquad \text{S1b.}$$

$$T'_\mathrm{do}\frac{\mathrm{d}\|\mathbf{v}_\mathrm{t}\|}{\mathrm{d}t} = -\|\mathbf{v}_\mathrm{t}\| + V_\mathrm{f} + \tfrac{X_d - X'_d}{V_\mathrm{t}} q_\mathrm{g}, \qquad \text{S1c.}$$

with scaled inertia constant $H = \frac{M\omega_0}{2S_\mathrm{base}}$, damping constant D, turbine power p_m, and grid power injection p_g expressed in per unit with base power S_base and base frequency ω_0. Moreover, $\|\mathbf{v}_\mathrm{t}\|$ and V_f denote the terminal voltage magnitude and output voltage of the exciter in per unit, T'_do denotes the time constant (i.e., ℓ/r) of the excitation winding, and X_d and X'_d denote static and transient d-axis reactances.

Frequency stability is commonly studied using the classical swing-equation model obtained by assuming that $\|\mathbf{v}_\mathrm{t}\|$ in Equation S1 is constant (i.e., using only Equations S1a and S1b). This assumption is commonly justified by the fact that T'_do is comparably large [i.e., on the order of seconds (15)]. While this prototypical model has proved itself useful (15, 22, 29), its validity has always been a subject of debate (see, e.g., 30–32).

We emphasize that any SG model needs to be combined with a suitable turbine model. While several specialized models for different turbine technologies exist (see, e.g., 15), the first-order turbine model

$$T_\mathrm{m}\frac{\mathrm{d}p_\mathrm{m}}{\mathrm{d}t} = -p_\mathrm{m} - K_\mathrm{gov}\omega \qquad \text{S2.}$$

with turbine time constant T_m and governor gain K_gov is commonly used for analyzing frequency stability and captures the main salient features of the turbine response (10, 29, 33).

2.2.2. DC/AC voltage source converter.

A DC/AC power converter converts signals and energy between its DC and AC ports. For a comprehensive modeling reference, we direct readers to Reference 16.

There are many topologies for power electronics conversion. To highlight similarities between SGs and voltage source converters (VSCs), we consider a basic VSC (depicted in **Figure 3**). The VSC converts a DC voltage $v_\mathrm{DC} \in \mathbb{R}$ and DC current $i_\mathrm{x} \in \mathbb{R}$ to a three-phase (in dq coordinates) AC voltage v_x and current $\mathbf{i}_\mathrm{f}$ (entering an inductive filter) according to

$$i_\mathrm{x} = \frac{1}{2}\mathbf{m}^\top \mathbf{i}_\mathrm{f} \quad \text{and} \quad \mathbf{v}_\mathrm{x} = \frac{1}{2}\mathbf{m} v_\mathrm{DC}, \qquad 10.$$

where $\mathbf{m} \in [-1, 1] \times [-1, 1]$ represents the averaged duty cycle ratio (16, chapter 5). This results in the averaged open-loop model

$$\begin{aligned} C_\mathrm{DC}\frac{\mathrm{d}v_\mathrm{DC}}{\mathrm{d}t} &= -G_\mathrm{DC}v_\mathrm{DC} + i_\mathrm{DC} - \frac{1}{2}\mathbf{m}^\top\mathbf{i}_\mathrm{f}, \\ L_\mathrm{f}\frac{\mathrm{d}\mathbf{i}_\mathrm{f}}{\mathrm{d}t} &= -(R_\mathrm{f}\mathcal{I} + \mathbf{J}\omega_0 L_\mathrm{f})\mathbf{i}_\mathrm{f} + \frac{1}{2}\mathbf{m}v_\mathrm{DC} - \mathbf{v}_\mathrm{t}, \end{aligned} \qquad 11.$$

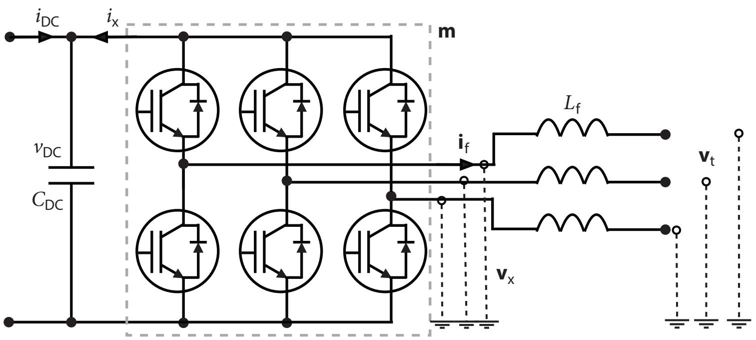

Figure 3

Two-level voltage source converter. A two-level voltage source converter with inductive filter uses semiconductor switches to modulate the DC voltage v_{DC} into the AC voltage v_{x}, and the AC filter current i_{f} into the DC current i_{x}.

where all parameters are as in **Figure 3**; G_{DC} and R_{f} model the lumped switching, charging, and conduction losses; $\mathbf{v}_{\mathrm{t}}$ is the AC voltage at the VSC terminals; and i_{DC} is the controllable DC-side current typically coming from an upstream converter (34, 35) or storage element.

Aside from an upstream power converter and power source, higher-order CIG models additionally consider inductive–capacitive (LC) or inductive–capacitive–inductive (LCL) filters at the AC terminals rather than a single inductor. There are also other converter topologies (i.e., arrangements of the switches in **Figure 3**), but the modeling is conceptually similar.

2.3. Modeling Fallacies in Low-Inertia Power Systems

The power system—all of its components and all of its operation—has been built around the central technology of the SG introduced in Section 2.2.1. A testimonial to this fact is the three-phase AC circuitry, which is due to the three-phase generation technology displayed in the SG's inductance matrix $\mathbf{L}_{\theta}$. Future low-inertia power systems will have a large share of CIG versus rotational generation, and hence conventional modeling assumptions, analysis, and control need to be revisited. In what follows, we comment on a few peculiarities of low-inertia systems and point out fallacies, where conventional models are misleading.

2.3.1. Time-domain versus quasi-steady-state models. The grid's circuitry has been derived in Equation 8. This model is of high fidelity but also cumbersome to simulate due to grid's vast size and the different timescales involved—e.g., the mechanical time constant of the SG model in Equation 9 is several orders slower than the circuit model in Equation 8. For these reasons, and since the stable passive circuit dynamics in Equation 8 are typically not of interest, the power system is usually modeled by differential-algebraic equations (36), where the network in Equation 8 is put into a quasi steady state (i.e., a steady state in a dq frame) and line flows are eliminated (26):

$$\mathbf{I}_{\mathrm{g}} - \mathbf{I}^{\star}_{\mathrm{load}} - \mathbf{G}(\mathbf{v}) \cdot \mathbf{v} = \mathbf{Y}\mathbf{v}, \qquad 12.$$

where $\mathbf{Y} = \mathbf{B}\mathbf{Z}^{-1}\mathbf{B}^{\top}$ is the network admittance matrix. Furthermore, these equations are formulated in units of power (by left-multiplying them by voltage), loads are typically modeled as constant power (or whatever is convenient for analysis) (37), bus voltages $\mathbf{v}_i$ are modeled as phasors $\mathbf{v}_i \sim \|\mathbf{v}_i\| e^{j\theta_i}$, and often voltages at buses without injections are eliminated using Kron reduction

(38). The active and reactive power balance at bus i is then

$$
\begin{aligned}
p_{i,\mathrm{g}} - p_{i,\mathrm{load}} &= \sum_{j\in\mathcal{V}} \|\mathbf{v}_i\|\|\mathbf{v}_j\| g_{ij}\cos(\theta_i-\theta_j) + \|\mathbf{v}_i\|\|\mathbf{v}_j\| b_{ij}\sin(\theta_i-\theta_j),\\
q_{i,\mathrm{g}} - q_{i,\mathrm{load}} &= \sum_{j\in\mathcal{V}} \|\mathbf{v}_i\|\|\mathbf{v}_j\| g_{ij}\sin(\theta_i-\theta_j) - \|\mathbf{v}_i\|\|\mathbf{v}_j\| b_{ij}\cos(\theta_i-\theta_j),
\end{aligned} \tag{13.}
$$

where $p_{i,\,\mathrm{g}}$ and $q_{i,\,\mathrm{g}}$ are the generator power injections defined implicitly via $\mathbf{I}_{i,\mathrm{g}} = \frac{1}{\|\mathbf{v}_i\|^2}\left(p_{i,\mathrm{g}}\mathcal{I} + q_{i,\mathrm{g}}\mathcal{J}\right)\mathbf{v}_i$, and g_{ij} and b_{ij} are the lossy and lossless admittances obtained as elements of the admittance matrix $Y = g\mathcal{I}_2 + \mathbf{J}b$.

The so-called power flow equations shown in Equation 13 are the foundation of power system steady-state analysis (26) and optimization (39), and they are typically used in conjunction with the SG model in Equation 9 for dynamic simulation, analysis, and control. The pivotal assumption underlying the quasi-steady-state power flow in Equation 13 is a timescale separation between line and SG dynamics, thus setting the time derivatives in Equation 8 to zero, as justified by singular perturbation methods (22). However, such an assumption is flawed with a large share of CIG: The dynamics of converters and their controls operate on a similar timescale as the line dynamics in Equation 8, which can result in resonance phenomena and ultimately instability (1, 5, 9, 40–42). Hence, either the full dynamic network model in Equation 8 must be taken into account, or one must be crucially aware of the limitations of the quasi-steady-state models in Equations 12 and 13. In fact, to avoid instability, power converter controllers are often deliberately slowed down or equipped with low-pass filters (for representative studies, see 43–47).

2.3.2. Similarities and differences of synchronous generator and voltage source converters. We now highlight the similarities and crucial differences of the SG and VSC devices from the viewpoint of energy conversion (48). Both devices can be understood as exchanging power between energy storage elements. The power balance across the SG in Equation 9 is given by

$$
\underbrace{\frac{\mathrm{d}}{\mathrm{d}t}\frac{1}{2}M\omega^2}_{\frac{\mathrm{d}}{\mathrm{d}t}\text{ mechanical energy}} + \underbrace{\frac{\mathrm{d}}{\mathrm{d}t}\frac{1}{2}\mathbf{i}_\mathrm{s}^\top L_\mathrm{s}\mathbf{i}_\mathrm{s}}_{\frac{\mathrm{d}}{\mathrm{d}t}\text{ magnetic energy}\approx 0} = \underbrace{-R_\mathrm{s}\|\mathbf{i}_\mathrm{s}\|^2 - D\omega^2}_{\text{electrical and mechanical losses}\approx 0} + \underbrace{\tau_\mathrm{m}\omega}_{\text{mechanical power}} + \underbrace{\mathbf{i}_\mathrm{s}^\top\mathbf{v}_\mathrm{t}}_{\text{AC power}}, \tag{14.}
$$

where the electromechanical energy conversion through the rotating magnetic field cancels out. Furthermore, the dissipation and magnetic energy terms are negligibly small, and thus the power balance is dominated by the large mechanical energy stored in the rotor as well as the electrical and mechanical power supply from the grid and the torque/governor system.

The power balance across the VSC in Equation 11 is given by

$$
\underbrace{\frac{\mathrm{d}}{\mathrm{d}t}\frac{1}{2}C_\mathrm{DC}v_\mathrm{DC}^2}_{\frac{\mathrm{d}}{\mathrm{d}t}\text{ DC energy}} + \underbrace{\frac{\mathrm{d}}{\mathrm{d}t}\frac{1}{2}\mathbf{i}_\mathrm{f}^\top L_\mathrm{f}\mathbf{i}_\mathrm{f}}_{\frac{\mathrm{d}}{\mathrm{d}t}\text{ magnetic energy}\approx 0} = \underbrace{-R_\mathrm{f}\|\mathbf{i}_\mathrm{f}\|^2 - G_\mathrm{DC}v_\mathrm{DC}^2}_{\text{switching and conduction losses}\approx 0} + \underbrace{i_\mathrm{DC}v_\mathrm{DC}}_{\text{DC power}} + \underbrace{\mathbf{i}_\mathrm{f}^\top\mathbf{v}_\mathrm{t}}_{\text{AC power}}, \tag{15.}
$$

where the DC–AC conversion through the modulation $\mathbf{m}$ cancels out. Furthermore, the dissipation and magnetic energy terms are typically negligibly small, and thus the power balance is dominated by the charge stored in the DC capacity as well as the AC and DC power supplies.

Hence, from an energy conversion viewpoint, both devices consist of a DC storage element (the rotating mass M or the DC capacitor C_DC) fed by a DC power supply (either mechanical $\tau_\mathrm{m}\omega$ or electrical $i_\mathrm{DC}v_\mathrm{DC}$) and a lossless DC–AC conversion (through the magnetic field L_θ or the modulation $\mathbf{m}$) to a negligible magnetic storage element and eventually the grid power supply ($\mathbf{i}_\mathrm{s}^\top\mathbf{v}_\mathrm{t}$ or $\mathbf{i}_\mathrm{f}^\top\mathbf{v}_\mathrm{t}$) (see **Figure 4**).

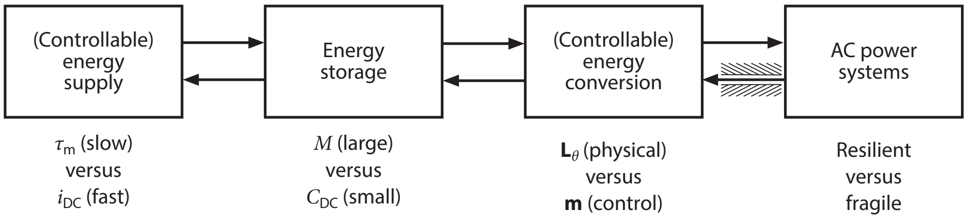

Figure 4

Voltage source converter and synchronous generator as energy-exchanging and DC–AC signal-transforming devices, respectively.

To further highlight the structural similarities, we parameterize the modulation $\mathbf{m}$ as

$$\mathbf{m} = u_{\text{mag}} \begin{bmatrix} -\sin\delta \\ \cos\delta \end{bmatrix} \quad \text{and} \quad \dot{\delta} = u_{\text{freq}}, \tag{16}$$

where $u_{\text{freq}} \in \mathbb{R}$ and $u_{\text{mag}} \in [-1, +1]$ are the controllable switching frequency and magnitude, respectively. With such a polar coordinate representation, the VSC dynamics in Equation 11 then read as

$$\begin{aligned} \frac{\mathrm{d}\delta}{\mathrm{d}t} &= u_{\text{freq}}, \\ C_{\text{DC}} \frac{\mathrm{d}v_{\text{DC}}}{\mathrm{d}t} &= -G_{\text{DC}} v_{\text{DC}} + i_{\text{DC}} + \frac{1}{2} u_{\text{mag}} \begin{bmatrix} -\sin\delta \\ \cos\delta \end{bmatrix}^\top \mathbf{i}_{\text{f}}, \\ L_{\text{f}} \frac{\mathrm{d}\mathbf{i}_{\text{f}}}{\mathrm{d}t} &= -(R_{\text{f}} + \mathbf{J}\omega_0 L_{\text{f}})\mathbf{i}_{\text{f}} + \mathbf{v}_{\text{g}} - \frac{1}{2} u_{\text{mag}} \begin{bmatrix} -\sin\delta \\ \cos\delta \end{bmatrix} v_{\text{DC}}. \end{aligned} \tag{17}$$

The VSC dynamics in Equation 17 now take an identical structure as the SG dynamics in Equation 9 after associating the DC voltage v_{DC} and capacitance C_{DC} with the SG rotational frequency ω and inertia M. The duality of mass and capacitance is well known to any engineering student, and it has informed multiple VSC control designs (2, 49–53) (see Section 3.4.4).

Despite these similarities, a closer look reveals several glaring and crucial differences. In particular, with regard to the time constants, typical time constants for the SG's mechanical power supply approximately range from, e.g., 3 s for hydro turbines to, e.g., 10 s for steam turbines, while the time constants of the VSC's DC power source approximately range from, e.g., 5 ms for photovoltaics to, e.g., 500 ms for pitch-controlled wind turbines. On the other hand, the SG rotor stores approximately 4–12 s of rated power, while the VSC DC link capacitor typically stores, e.g., 10–80 ms of rated power. Hence, for SGs, the actuation via the "DC power supply" is rather slow and inflexible, and the main "DC storage element" is very large, whereas for VSCs, the actuation via the "DC power supply" is very fast and flexible, and the main "DC storage element" is very small. Furthermore, for SGs, the "DC–AC conversion" is mostly physical, with little excitation control, and the grid connection is resilient (i.e., the converter's switches cannot tolerate any overcurrent), whereas for VSCs, the conversion is fully controlled via the modulation, and the grid connection is fragile. For these reasons, among others, it is shortsighted for VSC control to emulate an SG in closed loop (see Section 3.4.2).

In short, both devices are DC–AC signal and power transformers, the SG has large inherent energy storage but slow actuation, and the VSC is fully and quickly actuated but without significant storage. These similarities and differences inform the control design in Section 3.

2.3.3. Lingua franca between power systems and electronics. We close this section with some high-level thoughts. Until recently, power systems and power electronics engineers had few interactions and often spoke different languages. This fact is exemplified by how the two communities used to model each other's systems and devices. In the vast majority of scientific articles and teaching material in power electronics, the considered power system model is simply a stiff voltage source. In the power system world, by contrast, power converters have been typically modeled as constant or controllable current/voltage/power sources. Aside from the little interaction between the communities, this mutual disregard is simply due to the fact that there was no demand: The physics had little relevant interaction, and there were few operational requirements at the interface. However, as an increasing number of CIG sources were connected to the power system, various undesired phenomena emerged on both the grid side (e.g., subsynchronous oscillations) and the converter side (e.g., converters not being able to operate in the presence of a weak grid or withstand faults).

Our beliefs and observations are that control and systems theory can serve as the lingua franca that translates models and specifications between these two communities. Yet another bridging role of control is to enable CIG to be grid friendly, as discussed next.

3. CONTROL OF GRID-CONNECTED VOLTAGE SOURCE CONVERTERS

In this section, we review and broadly categorize prevalent and emerging control algorithms for grid-connected VSCs. In particular, we focus on the distinction between grid-following (GFL) control and grid-forming (GFM) control and the impact of the two control paradigms on system stability. We limit the discussion to the two-level VSC shown in **Figure 3**, with the understanding that the general ideas presented in this section can be extended to more advanced VSC topologies (see, e.g., 54).

3.1. Degrees of Freedom of Grid-Connected Voltage Source Converters

Before discussing the control objectives, we review the degrees of freedom of grid-connected two-level VSCs that inform their control objectives and design. Considering the modulated voltage and current in Equation 10, the active power supplied by CIG satisfies

$$p_{\mathrm{x}} = \mathbf{i}_{\mathrm{f}}^{\top}\mathbf{v}_{\mathrm{x}} = \mathbf{i}_{\mathrm{f}}^{\top}\frac{1}{2}\mathbf{m}v_{\mathrm{DC}} = \frac{1}{2}\mathbf{m}^{\top}\mathbf{i}_{\mathrm{f}}v_{\mathrm{DC}} = i_{\mathrm{x}}v_{\mathrm{DC}}, \qquad 18.$$

and, using $p_{\mathrm{DC}} = v_{\mathrm{DC}}i_{\mathrm{DC}}$, the DC capacitor charge dynamics in Equation 11 can be rewritten as

$$\tfrac{\mathrm{d}}{\mathrm{d}t}\tfrac{1}{2}C_{\mathrm{DC}}v_{\mathrm{DC}}^2 = -G_{\mathrm{DC}}v_{\mathrm{DC}}^2 + p_{\mathrm{DC}} - p_{\mathrm{x}}. \qquad 19.$$

In other words, the DC energy $E_{\mathrm{DC}} = \frac{1}{2}C_{\mathrm{DC}}v_{\mathrm{DC}}^2$ can be directly controlled through the DC power p_{DC} and/or active power p_{x}. By contrast, $q_{\mathrm{x}} = \mathbf{i}_{\mathrm{f}}^{\top}\mathbf{J}\mathbf{v}_{\mathrm{x}}$ corresponds to currents that circulate through the switches and AC phases but do not reach the DC side (i.e., are orthogonal to $\mathbf{v}_{\mathrm{x}}$). Note that a two-level VSC can only modulate AC voltages with magnitude $\|\mathbf{v}_{\mathrm{x}}\| \leq \frac{1}{2}v_{\mathrm{DC}}$ and needs to be able to impose voltage magnitudes $\|\mathbf{v}_{\mathrm{x}}\| \geq \|\mathbf{v}_{\mathrm{g}}\|$ to fully control its power injection (see Equation 13). In this case, the reactive power q_{g} can be controlled without affecting DC voltage v_{DC} because $q_{\mathrm{x}} = \mathbf{i}_{\mathrm{f}}^{\top}\mathbf{J}\mathbf{v}_{\mathrm{x}}$ corresponds to currents that circulate through the switches and AC phases but do not reach the DC side (i.e., $\mathbf{i}_{\mathrm{f}}$ is orthogonal to $\mathbf{v}_{\mathrm{x}}$). Moreover, assuming a lossless filter in quasi steady state, p_{x} and q_{x} are equal to the grid power injections $p_{\mathrm{g}} = \mathbf{i}_{\mathrm{f}}^{\top}\mathbf{v}_{\mathrm{t}}$ and $q_{\mathrm{g}} = \mathbf{i}_{\mathrm{f}}^{\top}\mathbf{J}\mathbf{v}_{\mathrm{t}}$, respectively, given by the power flow in Equation 13.

3.2. Control Objectives and Control Paradigms

We now provide an overview of control objectives and paradigms for grid-connected VSCs.

3.2.1. Control objectives. Before presenting common control objectives, we note that there is no precise and universally agreed-upon framework for dynamic specifications for grid-connected VSCs. Instead, control objectives for grid-connected VSCs are commonly formulated in terms of decentralized stabilization (i.e., using only local measurements) of a nominal steady state specified by the following:

- Synchronous frequency (22, 55): All AC signals are balanced periodic three-phase signals with nominal frequency ω_0.
- Power injection (47, 56): Each VSC injects the prescribed active and reactive power—i.e., $(p_g, q_g) = (p_g^\star, q_g^\star)$.
- AC voltage magnitude (22, 57): Given a nominal AC voltage magnitude $V_t^\star$, it holds that $\|\mathbf{v}_t\| = V_t^\star$.
- DC voltage (35, 49): Given a nominal DC voltage $v_{DC}^\star$, it holds that $v_{DC} = v_{DC}^\star$.

We emphasize that the nominal operating point $(\omega_0, v_{DC}^\star, p_g^\star, q_g^\star, V_t^\star)$ needs to correspond to a steady state of the power network, power conversion (e.g., SGs and VSCs), and power generation (55, 58). For example, the power injections $(p_g^\star, q_g^\star)$ and voltage magnitude $V_t^\star$ need to be consistent with the AC power flow in Equation 13 (see, e.g., 26). Typically, the operating point may be (partially) prescribed by a system operator based on solutions of an optimal power flow (58) or local control objectives such as maximum power point tracking for renewable generation (34, 35). However, due to disturbances (i.e., variations in load or generation or faults), the nominal operating point may not correspond to an equilibrium of the power system. For example, considering the power balance in Equation 14, one can see that the frequency will deviate due to mismatches in load and generation. In this case, one or more of the signals must deviate from the nominal operating point to stabilize the VSC and overall system at a synchronous solution with identical non-nominal frequency at every bus (i.e., $\omega_1 = \omega_2 = \cdots = \omega_n$) and with minimal transients (22, 59, 60).

Next, we focus on common specifications for the steady-state disturbance response. Historically, a large part of the literature has focused on controlling the DC voltage v_{DC} to a setpoint $v_{DC}^\star$ [e.g., the maximum power point of photovoltaics (35) or the nominal voltage of an HVDC cable (61)] at all times. In this case, the current i_{DC} or power p_{DC} is treated as an exogenous input [e.g., renewable generation operating at its maximum power point (34, 35) or current flowing into an HVDC network (61)]. Crucially, if p_{DC} is an exogenous input, the DC voltage dynamics in Equation 19 can be controlled only through $p_x \approx p_g$—i.e., the active power p_g is prescribed largely by the DC source power p_{DC}.

By contrast, for VSCs providing grid support (62), the steady-state disturbance response is typically designed to mimic the steady-state droop response of the classical SG turbine (see Equation S2 in the sidebar titled Reduced-Order Synchronous Generator and Turbine Models) and SG excitation system (see Equation S1c). This results in the so-called frequency–watt droop (56, 59) and volt-var droop (56, 57),

$$\omega - \omega_0 = m_p \cdot (p_g^\star - p_g) \qquad \text{and} \qquad \|\mathbf{v}_t\| - V_t^\star = m_q \cdot (q_g^\star - q_g), \tag{20.}$$

which trade off AC voltage frequency and magnitude deviations with active and reactive power deviations according to the droop coefficients m_p and m_q (56). If frequency–watt droop is used, it is commonly assumed that the DC voltage v_{DC} is stabilized by controlling the VSC power source (i.e., p_{DC}). Irrespective of how v_{DC} is controlled, the reactive power q_g can be varied within the converter power limits (16, 56).

We emphasize that grid-supporting VSC controls are designed to mimic the response of the classical third-order SG model in Equation S1, and the specifications presented in this section are obtained by reverse engineering this response. To the best of our knowledge, so-called dispatchable virtual oscillator control (dVOC) (see Section 3.4.3) is the only principled control approach designed starting from precise specifications (47, 63).

3.2.2. Control paradigms. In the literature, control strategies for grid-connected VSCs are typically categorized as GFL or GFM. We emphasize that there is no precise and universally agreed-upon definition of GFL and GFM across different research communities. According to early definitions used in power electronics, a GFM VSC acts as a voltage source (i.e., it imposes an AC voltage with constant nominal amplitude and frequency), while a GFL VSC acts as current or power source (i.e., it injects a controllable power) (56). Nowadays, GFM often refers to a VSC that imposes an AC voltage with a frequency that is adjusted to ensure frequency synchronization and provide grid support. By contrast, GFL is often used to describe a VSC that relies on a so-called phase-locked loop (PLL) for synchronization and current control irrespective of whether further grid-support functions are implemented (64). Other definitions encountered in the power systems literature hinge on the presence of virtual inertia, the ability of the VSC to operate islanded with load, or the ability to suppress frequency oscillations (65). While the classification into GFL and GFM commonly refers to the converter AC terminal, it is also useful to characterize a VSC as DC-GFL if it relies on a stable DC voltage and as DC-GFM if it imposes a stable DC voltage (61).

To highlight the main distinction between GFL and GFM control, we refer henceforth to a VSC as AC-GFM (or DC-GFM) if it imposes a stable, well-defined AC (DC) voltage at the AC (DC) converter terminal, and as AC-GFL (or DC-GFL) if the control crucially hinges on the assumption that a well-defined AC (DC) voltage at the VSC AC (DC) terminal is guaranteed a priori by the presence of other generation units. Prototypical implementations of standard AC-GFL/DC-GFM and AC-GFM/DC-GFL control, as well as recently developed AC-GFM/DC-GFM control, are shown in **Figure 5**.

3.3. AC Grid-Following Control of Voltage Source Converters

The prevalent control for grid-connected renewable generation and energy storage today is AC-GFL control that uses a PLL [i.e., a proportional–integral (PI)–type observer] to estimate the terminal voltage phase angle $\angle \mathbf{v}_{\mathrm{t}}$ (see, e.g., 66) and control the VSC current $\mathbf{i}_{\mathrm{f}}$ in the corresponding *dq* frame (34, 35, 56). Specifically, the current $\mathbf{i}_{\mathrm{f}}$ is controlled through feedback linearization (i.e., $\mathbf{m} = \frac{2}{v_{\mathrm{DC}}}\mathbf{v}_{\mathrm{x}}^{\star}$) and PI control, denoted by $G_{\mathrm{PI}}(s)$ (56, 67),

$$\mathbf{v}_{\mathrm{x}}^{\star} = (R_{\mathrm{f}}\mathcal{I} + \mathbf{J}\omega_0 L_{\mathrm{f}})\mathbf{i}_{\mathrm{f}} + \mathbf{v}_{\mathrm{t}} + G_{\mathrm{PI}}(s)\,(\mathbf{i}_{\mathrm{f}}^{\star} - \mathbf{i}_{\mathrm{f}}), \tag{21}$$

such that, with a slight abuse of notation, the closed-loop filter current dynamics in Equation 11 become $L_{\mathrm{f}}\frac{\mathrm{d}\mathbf{i}_{\mathrm{f}}}{\mathrm{d}t} = G_{\mathrm{PI}}(s)(\mathbf{i}_{\mathrm{f}}^{\star} - \mathbf{i}_{\mathrm{f}})$. This PLL-based current control requires (*a*) a strongly coupled AC system to ensure that the VSC terminal voltage $\mathbf{v}_{\mathrm{t}} = \mathbf{v}_{\mathrm{g}}$ is largely independent of the converter current $\mathbf{i}_{\mathrm{f}}$ (see, e.g., 67; 16, chapter 8) as well as (*b*) AC-GFM units that impose stable AC voltage waveforms. In practice, these assumptions are often questionable and jeopardize system reliability and resilience. In particular, various instability mechanisms can arise, ranging from frequency instability to positive feedback induced by the PLL (5, 67). To the best of our knowledge, analytic stability certificates for AC-GFL have not been extended beyond the setting of VSCs without DC-side dynamics connected to an infinite bus (see, e.g., 67, 68). Nonetheless, the PLL-based current control is the basis for prototypical AC-GFL/DC-GFM controls used to control the DC voltage of VSCs interfacing with renewable generation (34, 35) and HVDC transmission (61). Specifically, considering the DC capacitor dynamics in Equation 19, the current $\mathbf{i}_{\mathrm{f}}^{d\star}$ and active power $p_{\mathrm{x}} \approx \|\mathbf{v}_{\mathrm{g}}\|\mathbf{i}_{\mathrm{f}}^{d\star}$ flowing out of the DC link capacitor can be used to control the DC voltage (34, 35).

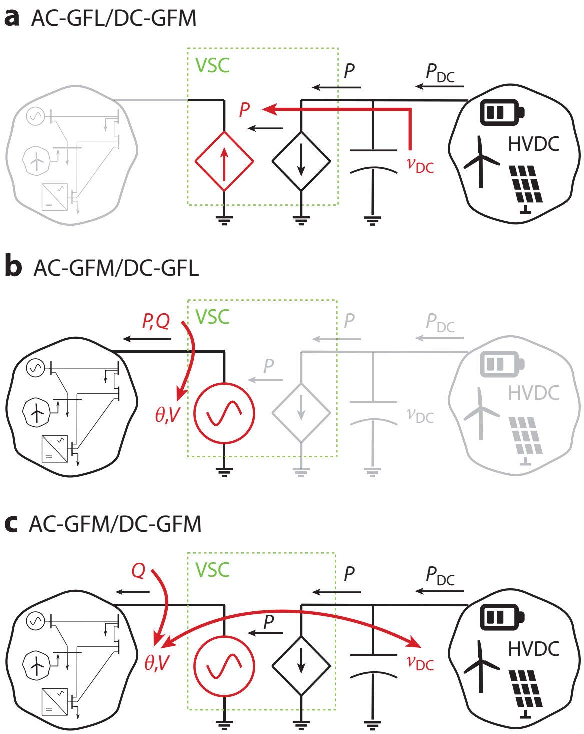

Figure 5

Signals imposed/controlled by a VSC (*red*) and components neglected in the control design (*gray*) for (*a*) a typical AC-GFL/DC-GFM control, which assumes a stable AC voltage and stabilizes the DC voltage and DC source; (*b*) a typical AC-GFM/DC-GFL control, which assumes a stable DC voltage and imposes a stable AC voltage; and (*c*) AC-GFM/DC-GFM control, which imposes a stable AC voltage but varies the AC voltage frequency to stabilize the DC voltage and DC source. Abbreviations: GFL, grid-following; GFM, grid-forming; HVDC, high-voltage DC; VSC, voltage source converter.

Finally, a wide body of literature exists on AC-GFL/DC-GFL controls that assume a constant DC voltage and compute the current reference $\mathbf{i}_{\mathrm{f}}^{\star}$ using $\mathbf{i}_{\mathrm{f}}^{d\star} = p_{\mathrm{g}}/\|\mathbf{v}_{\mathrm{g}}\|$, $\mathbf{i}_{\mathrm{f}}^{q\star} = q_{\mathrm{g}}/\|\mathbf{v}_{\mathrm{g}}\|$, as well as p_{g} and q_{g} obtained from the droop characteristic in Equation 20 and PLL estimates of the grid frequency and AC voltage magnitude (56, 69). However, in our view and that of an ever-growing part of the community, AC-GFL/DC-GFL control does not offer any advantage over the AC-GFM/DC-GFL controls discussed in the next section, while inheriting the aforementioned stability and resilience concerns related to the PLL (62, 64, 67).

3.4. AC Grid-Forming Control of Voltage Source Converters

In contrast to the AC-GFL control discussed in the previous section, AC-GFM power converters contribute to grid stabilization and are envisioned to be the cornerstone of future sustainable, reliable, and resilient low-inertia power systems (1, 9, 64). However, the prevalent AC-GFM control methods may fail if the DC voltage is not tightly controlled by the DC power source (10)—i.e., they are DC-GFL. In this section, we describe AC-GFM control architectures with and without inner control loops, and discuss the similarities and differences among three different classes of AC-GFM controls.

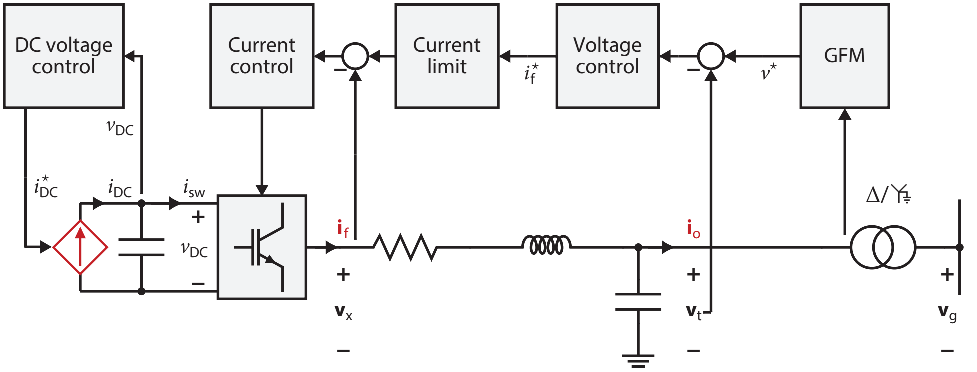

Figure 6

Standard AC-GFM control architecture with cascaded inner loops and controllable DC source. The inner current and voltage control loops control the filter current and voltage to track the AC-GFM voltage reference v_{GFM} provided by the outer GFM control. Abbreviation: GFM, grid-forming.

3.4.1. Grid-forming control architectures. Broadly speaking, standard AC-GFM control measures the VSC AC current or AC power and adjusts the VSC AC voltage to achieve the control objectives discussed in Section 3.2.1. To this end, the AC-GFM control either directly adjusts the voltage $\mathbf{v}_x$ modulated by the VSC or provides a reference for the LCL filter voltage that is tracked by an underlying cascaded current and voltage controller, as shown in **Figure 6**. While direct control of $\mathbf{v}_x$ has received some attention in the literature (49, 53, 64, 70, 71), the vast majority of works use cascaded PI controls that suppress LCL filter resonances through control of $\mathbf{v}_t$, increase the bandwidth, and provide a simple surrogate for overcurrent protection by limiting the AC current reference $\mathbf{i}_f^{\star}$ (46, 56, 72–74). While these features are appealing, it should be noted that the inner control loops need to be carefully tuned to account for the strength of the grid coupling to avoid instability (46, 70, 75). In addition, the timescale separation of cascaded control loops can result in a loss of control bandwidth and suboptimal response (70, 76).

Moreover, limiting the AC current reference can result in a loss of synchronization or synchronous instability (10, 77, 78) and complicates model reduction (74) (for an in-depth discussion of current-limiting strategies, see 74, 77–80). Next, we focus on the dynamics of the AC-GFM voltage reference $\mathbf{v}_{GFM}$ with the understanding that it can be used with (i.e., $\mathbf{v}_t \approx \mathbf{v}_{GFM}$) and without (i.e., $\mathbf{v}_x = \mathbf{v}_{GFM}$) inner controls.

3.4.2. Droop control and virtual synchronous machines. The prevalent approaches to AC-GFM control in the literature are so-called droop control (56, 81, 82) and virtual synchronous machines (VSMs) (73, 83). Both controls assume a constant nominal DC voltage (i.e., AC-GFM/DC-GFL). Droop control is motivated by the observation that, in steady state, the frequency deviation of the SG is proportional to its active power injection and the voltage magnitude is proportional to its reactive power injection. Moreover, in an inductive network, the active power is approximately proportional to the voltage phase angle differences and the reactive power is approximately proportional to the voltage magnitude (see Equation 13). In other words, the machine dynamics result in frequency synchronization through the network (59, 84) and active and reactive power sharing (57, 59). Hence, voltage magnitude and frequency drooping as in Equation 20 is an integral part of many grid codes.

These observations motivate using feedback of the VSC active power injection p_g to determine the phase angle $\theta = \angle \mathbf{v}_{GFM}$ and frequency of the AC-GFM reference voltage $\mathbf{v}_{GFM}$ and feedback of the VSC reactive power injection q_g to determine its magnitude $\|\mathbf{v}_{\text{GFM}}\|$. In particular, AC-GFM droop control is obtained by letting $H = 0$, $T_m = 0$, and $T'_{do} = 0$ in the one-axis SG model with exciter in Equation S1. Linearizing the resulting expression at the nominal terminal voltage magnitude (i.e., one per unit) and replacing the SG power injections with low-pass-filtered measurements $\tilde{p}_g = \frac{1}{\tau_{lp}s+1} p_g$ and $\tilde{q}_g = \frac{1}{\tau_{lp}s+1} q_g$ (e.g., to remove switching harmonics and set the bandwidth to avoid adverse interactions; see Section 2.3.1) gives

$$\frac{d\theta}{dt} = \omega_0 + m_p \cdot (p^\star - \tilde{p}_g) \qquad \text{and} \qquad \|\mathbf{v}_{\text{GFM}}\| = V^\star + m_q \cdot (q^\star - \tilde{q}_g) \tag{22.}$$

with droop gains m_p and m_q and power setpoints $p^\star$ and $q^\star$. While the droop gains are typically prescribed through grid codes and markets and typically range from 1% to 5%, we note that the equivalent droop gains of the one-axis SG model with exciter are $m_p = 1/(D + K_{\text{gov}})$ and $m_q = X_d - X'_d$. Finally, we note that all of the GFM controllers below will admit an explicit or implicit drooping behavior akin to Equation 22.

Similar to droop control, a wide range of VSM controls have been proposed to mimic SG models, such as the one-axis model with exciter in Equation S1 and the swing-equation model (see, e.g., 69, 73, 83, 85). In light of the fast actuation capabilities of VSCs and typical power sources, emulating the slow response of the turbine and excitation winding would artificially slow down the VSC response. In particular, letting $T_m = 0$ and $T'_{do} = 0$ in the one-axis SG model with exciter in Equation S1, linearizing at the nominal terminal voltage magnitude, and replacing q_g with the filtered measurement $\tilde{q}_p$ results in

$$\frac{2H}{\omega_0}\frac{d\omega}{dt} = -D\omega + p^\star - p_g, \qquad \|\mathbf{v}_{\text{GFM}}\| = V^\star + m_q \cdot (q^\star - \tilde{q}_g), \tag{23.}$$

with virtual inertia constant H and damping D. We emphasize that the limited internal energy storage and overload capability of VSCs precludes emulating a significant inertia constant H (10). In addition, most practical implementations of Equations 22 and 23 rely on auxiliary controls (e.g., virtual impedance, PLL-based damping, or inner controls) and are not exact analogues to SGs. Finally, we note that AC-GFM droop control in Equation 22 and the VSM in Equation 23 are identical up to a change of coordinates (84) and that the equivalent inertia constant $\frac{2H}{\omega_0} = \tau_{lp}/m_p$ of AC-GFM droop control in Equation 22 is typically small (see **Figure 7** and, e.g., References 84 and 86).

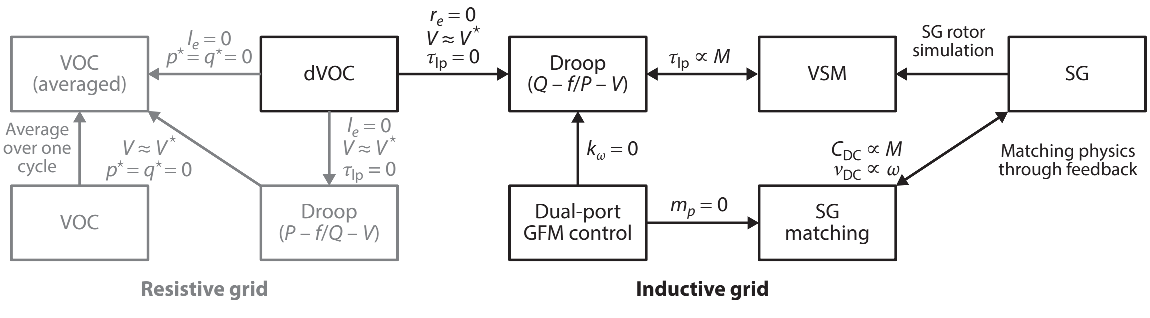

Figure 7

Classification and implications of different AC-GFM controls. AC-GFM controls can be broadly categorized into controls for predominantly inductive (i.e., transmission) and predominantly resistive (i.e., distribution and microgrids) systems. dVOC subsumes both cases, and the controls in each category coincide under a suitable choice of parameters and coordinates. Abbreviations: dVOC, dispatchable virtual oscillator control; GFM, grid-forming; SG, synchronous generator; VOC, virtual oscillator control; VSM, virtual synchronous machine.

Conceptually, the equivalence between droop control in Equation 22, the VSM in Equation 23, and the SG swing-equation model in Equation 9 ensures a basic level of interoperability between droop-controlled VSCs, VSMs, and SGs. Moreover, in principle, the vast literature on transient stability analysis for reduced-order SG models (see, e.g., 87, 88) can be readily applied to droop-controlled VSCs and VSMs. However, despite decades of research, general (almost or semi) global stability results for networks of SGs interconnected through the dynamic network model in Equation 8 or the quasi-steady-state model in Equation 13 have remained elusive. Standard results for local asymptotic stability typically assume a lossless network (i.e., $g_{ij} = 0$) and constant voltage magnitudes, apply only to the trivial (i.e., zero power flow) solution, and do not extend to a dynamic network model. Notable results include stability conditions for (*a*) linearizations around the zero power flow solution with network dynamics (45); (*b*) $\tau_{\mathrm{lp}} = 0$, the nonlinear quasi-steady-state network model in Equation 13 with no losses, and general synchronous solutions (60); and (*c*) linearizations around nontrivial operating points, lossy quasi-steady-state network models, and constant voltage magnitudes (89).

3.4.3. Virtual oscillator control.

A seemingly independent class of AC-GFM/DC-GFL controls is so-called virtual oscillator control (VOC) (47, 63, 90–94). While initial works on VOC focused on stand-alone uninterruptible power supplies (90), follow-on works leveraged the self-synchronization of nonlinear oscillators to control networks of single-phase converters (91–93, 95). More recent works have focused on enabling VOC control for three-phase VSCs to track a nominal operating point (47, 63). In contrast to droop control and VSMs, (almost) global synchronization certificates are available for networks of VOC-controlled VSCs (92, 93). Moreover, robust synchronization is observed in practice (92), and averaging VOC over one cycle (95) recovers droop control for resistive networks (56).

However, for all of the above VOC implementations, the nominal power injection cannot be dispatched, and the power sharing by the VSCs and their voltage magnitudes are determined by the load and network parameters. This lack of control over the network's operating point is highly problematic in large-scale systems that are coordinated through system-level controls and market mechanisms. This challenge is resolved in dVOC, a principled control approach combining a harmonic oscillator with a synchronizing feedback and magnitude control (47, 63). In stationary $\alpha\beta$ coordinates, the dVOC reference voltage v_{GFM} is given by

$$\underbrace{\frac{\mathrm{d}v_{\mathrm{GFM}}}{\mathrm{d}t} = \omega_0 \mathcal{J} v_{\mathrm{GFM}}}_{\text{harmonic oscillation at } \omega_0} + \underbrace{\eta \left[K v_{\mathrm{GFM}} - R(\kappa)\mathbf{i}_{\mathrm{o}}\right]}_{\text{synchronization through current}} + \underbrace{\eta\alpha\Phi(v_{\mathrm{GFM}})v_{\mathrm{GFM}}}_{\text{voltage magnitude control}}, \qquad 24.$$

with synchronization gain $\eta \in \mathbb{R}_{>0}$, magnitude control gain $\alpha \in \mathbb{R}_{>0}$,

$$K = \frac{1}{V^\star V^\star} R(\kappa) \begin{bmatrix} p_{\mathrm{g}}^\star & q_{\mathrm{g}}^\star \\ -q_{\mathrm{g}}^\star & p_{\mathrm{g}}^\star \end{bmatrix}, \qquad \text{and} \qquad \Phi(v_{\mathrm{GFM}}) \frac{V^\star V^\star - \|v_{\mathrm{GFM}}\|^2}{V^\star V^\star}.$$

Here, $R(\kappa)$ denotes the 2D rotation matrix, and $\kappa \tan^{-1}(\omega_0 \cdot \ell/r)$ denotes the ℓ/r ratio of the network, which is approximately constant for transmission lines at the same voltage level. dVOC has several appealing features. First, the nominal operating point of dVOC can be defined through setpoints $(V^\star, p_{\mathrm{g}}^\star, q_{\mathrm{g}}^\star)$, as for droop or VSM controllers. Second, almost global stability certificates are available for dynamic networks (see Equation 8) with uniform ℓ/r ratio, LC filter dynamics, and inner control loops that provide bounds on the network connectivity, network loading, and timescale separation between control loops and the network dynamics (46). Third, dVOC can be understood as a generalization of droop control and VOC to more general networks (for classifications and implications, see **Figure 7**). In particular, for inductive networks (i.e., transmission systems), and assuming near-nominal voltage magnitudes, dVOC resembles droop control (96). By contrast, for resistive networks (i.e., microgrids) and $p_{\mathrm{g}}^{\star} = q_{\mathrm{g}}^{\star} = 0$, dVOC is identical to averaged VOC (63). Notable recent works include unified virtual oscillator control (uVOC), which provides AC-GFL functions and fault ride-through capabilities (97).

3.4.4. Machine matching and dual-port grid-forming control.

So far, we have discussed AC-GFM/DC-GFL controls that neglect the DC voltage dynamics (i.e., assume that $v_{\mathrm{DC}} = v_{\mathrm{DC}}^{\star}$). By contrast, so-called machine emulation or machine matching control (49, 51, 53, 71) leverage the similarities between DC voltage and synchronous machine frequency as indicators of power imbalances (see Equations 14 and 15 as well as Equations 9 and 17). In particular, using $\frac{\mathrm{d}\theta}{\mathrm{d}t} = \omega$,

$$\omega = k_{\omega} v_{\mathrm{DC}}, \tag{25}$$

$\mathbf{m}$ in $\alpha\beta$ coordinates is given by $\mathbf{m} = u_{\mathrm{mag}}\left[\begin{smallmatrix} -\sin\theta \\ \cos\theta \end{smallmatrix}\right]$ (see Section 2.3.2). Using this control, the SG dynamics in Equation 9 and VSC dynamics in Equation 11 coincide with the inertia constant $M = \frac{C_{\mathrm{DC}}}{k_{\omega}^2}$, damping constant $D = \frac{G_{\mathrm{DC}}}{k_{\omega}^2}$, and torque $\tau_{\mathrm{m}} = \frac{i_{\mathrm{DC}}}{k_{\omega}}$ (49). The relationships among different AC-GFM controls and SGs are illustrated in **Figure 7**. In contrast to the VSMs discussed above, the two models are exactly structurally equivalent. However, the inertia and damping constants of the equivalent SG are typically significantly smaller than those of an SG with comparable rating and can result in poorly damped dynamics. Moreover, the controller in Equation 25 again leads to the challenging problem of analyzing the stability of multimachine systems.

An often overlooked feature of the control in Equation 25 is that it is AC-GFM and ensures power balancing between the DC and AC terminal of the VSC by controlling the DC voltage through the AC terminal. The resulting AC-GFM/DC-GFM control can operate if either the AC or DC voltage is stabilized by another AC-GFM or DC-GFM device. In particular, if the DC voltage (AC voltage frequency) is stabilized by a DC-GFM source (AC-GFM) device, then the AC voltage frequency (DC voltage) is also stable. This observation has led to the development of so-called dual-port GFM control (54, 98), which combines active power droop in Equation 22 with a DC voltage droop term (98),

$$\omega - \omega_0 = m_p \cdot \left(p^{\star} - p_{\mathrm{g}}\right) + k_{\omega} \cdot \left(v_{\mathrm{DC}} - v_{\mathrm{DC}}^{\star}\right), \tag{26}$$

and unifies standard functions of AC-GFM (e.g., primary frequency control) and AC-GFL (e.g., maximum power point tracking) control in a single universal controller without mode switching or PLL. Moreover, the dual-port GFM control in Equation 26 enables an end-to-end linear stability analysis accounting for AC and DC transmission, SGs and VSCs with and without controlled generation, and generic models of conventional and renewable generation (98).

3.5. Grid-Forming Control as the Cornerstone of Low-Inertia Systems

We close this section with some high-level thoughts on the role of AC-GFM and AC-GFL converters in future low-inertia power systems. The two approaches are complementary in the sense that AC-GFM/DC-GFL requires a fully controllable power source (e.g., energy storage) and has a significant positive impact on system stability, damping, and resilience (5, 8, 10, 62, 64), while AC-GFL/DC-GFM requires a stable AC grid (e.g., the presence of AC-GFM units) and stabilizes CIG. Notably, standard AC-GFL control is vulnerable to instability due to grid disturbances (99), weak grid coupling (67), and massive integration of AC-GFL converters (5, 67). On the other hand, at present, AC-GFM control may fail due to limited power source controllability (10) and/or converter current limits (10, 77, 78). Given the clear need for AC-GFM CIG, incorporating converter (e.g., current and modulation limits) and power source dynamics and limitations (e.g., power and bandwidth limits) directly into the design of AC-GFM controls is an important topic for future research. Similarly, multiple-input and multiple-output (MIMO) controls that generalize and unify the various AC-GFM approaches can result in significantly improved dynamic performance (100, 101).

Moreover, at present, a mix of AC-GFL/DC-GFM and AC-GFM/DC-GFL control is needed to operate emerging power systems that contain renewable generation (34, 35) and/or HVDC transmission (61). The resulting complex, heterogeneous system dynamics—which combine the network dynamics in Equation 8, the dynamics of the energy conversion devices in Equations 9 and 11, the dynamics of conventional and renewable generation, and AC-GFM and AC-GFL controls—pose significant challenges for power system operation and stability analysis (5). Ultimately, the dynamics of emerging technologies, such as HVDC, wind turbines, and energy storage systems (e.g., batteries and flywheels), that are interfaced by VSCs need to be accounted for to certify end-to-end stability (i.e., from power generation to load) instead of merely certifying the stability of a network of AC-GFM converters with constant DC voltage. Machine matching and dual-port GFM controls are a promising approach to tackle this challenge and reduce the system complexity by unifying AC-GFL and AC-GFM control (98).

4. LOW-INERTIA FREQUENCY DYNAMICS AND CONVERTER-INTERFACED GENERATION INTEGRATION LIMITS

The previous section focused on control of grid-connected VSCs and the positive impact of AC-GFM control on power system stability and resilience compared with the predominantly negative impact of AC-GFL control. On the other hand, from a practical point of view, the discussion of the transition to a power system with massive integration of CIG often focuses on the so-called loss of rotational inertia due to retiring SGs (3, 4, 7, 102). However, the challenges of this transition related to control and dynamic stability are significantly more nuanced (5, 8, 10). In this section, we briefly review typical models and metrics for frequency dynamics of multimachine systems, revisit the role of inertia in low-inertia power systems, and discuss open research questions that limit the integration of CIG into today's large-scale systems.

4.1. Frequency Stability in Multimachine and Low-Inertia Systems

In power engineering, the frequency dynamics of conventional SG-based power systems are often decomposed into the so-called center of inertia (COI) frequency $\omega_{\mathrm{COI}} = \sum_{k=1}^{n_m} H_k \omega_k / H_{\mathrm{tot}}$, with total system inertia $H_{\mathrm{tot}} = \sum_{k=1}^{n_m} H_k$ and deviation of the individual machine angles θ_k and frequencies ω_k from the COI frequency ω_{COI} (22, 29). For homogeneous SGs (i.e., whose inertia and damping constants are proportional to the SG rating and turbine time constants are identical), the small-signal dynamics of the COI frequency and angle/frequency deviations decouple (29) and can be analyzed in isolation. For brevity of presentation, we focus on the COI frequency dynamics and direct readers to Reference 29 for a detailed analysis of the deviation from synchrony.

The COI frequency ω_{COI} dynamics are commonly modeled by a single equivalent swing-equation model (i.e., Equation S1b) with total system inertia $H = H_{\mathrm{tot}}$, negligible damping D, a first-order turbine model (Equation S2) with aggregate turbine time constant $T_{\mathrm{m}} = T_{\mathrm{agg}}$ (33), and total primary frequency control gain $K_{\mathrm{gov}} = K_{\mathrm{tot}}$ in per unit (22). The response of the COI model in Equation S1b with Equation S2 to a step in active power p_{g} is shown in **Figure 8**. From a power engineering point of view, the rate of change of frequency (RoCoF) and frequency nadir (i.e., its minimum) are key performance metrics.

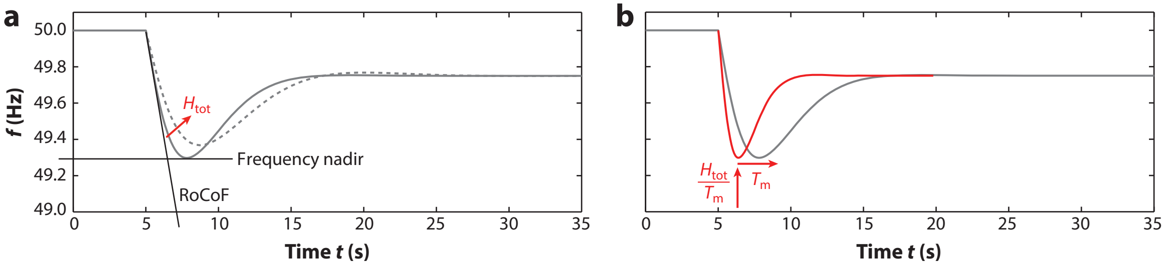

Figure 8

Response of the COI dynamics to a load step. (*a*) Increasing the inertia H_{tot} results in a decreased RoCoF and frequency nadir. (*b*) A system with a larger aggregate turbine time constant T_{agg} evolves on a slower timescale, and increasing the ratio $H_{\text{tot}}/T_{\text{agg}}$ results in a reduced nadir. Abbreviations: COI, center of inertia; RoCoF, rate of change of frequency.

Before proceeding, we emphasize that the COI frequency ω_{COI} is a fictitious frequency that all SGs would synchronize to in steady state. However, power systems are subject to persistent disturbances (e.g., load fluctuations), and the individual machine frequencies ω_k never settle to the COI frequency ω_{COI}. Thus, ensuring frequency coherency (i.e., small deviations from synchrony) and suppressing interarea oscillations (see, e.g., 103) are important system-level objectives. Moreover, in systems of heterogeneous SGs, the spatial distribution of inertia and damping has a significant impact (for further discussion, see Section 5).

Conventional wisdom suggests that replacing SGs with CIG without virtual inertia results in a reduction of the total inertia H_{tot} and, according to the COI model, an increased RoCoF and frequency nadir (3, 4, 29, 102). However, the kinetic energy stored in the SG rotor merely acts as an energy buffer until the SG turbine responds. Using the AC-GFM controls discussed in the previous section, CIG without virtual inertia responds to power imbalances on timescales of milliseconds—i.e., both H_{tot} and the aggregate turbine time constant T_{agg} are reduced. To clarify the impact of this change, note that rescaling time in the COI model does not change the frequency nadir. With $t' = T_{\text{agg}} t$, Equations S1b and S2 become

$$\frac{2H_{\text{tot}}}{\omega_0 T_{\text{m}}} \frac{\mathrm{d}\omega}{\mathrm{d}t'} = -D\omega + p_{\text{m}} - p_{\text{g}}, \qquad \frac{\mathrm{d}p_{\text{m}}}{\mathrm{d}t'} = -p_{\text{m}} - K_{\text{tot}}\omega\,. \qquad 27.$$

Standard arguments (29) can be used to show that the frequency nadir is a decreasing function of $H_{\text{tot}}/T_{\text{agg}}$. In other words, using AC-GFM CIG, the frequency dynamics of the power system evolve on faster timescales, and less inertia is required. While the maximum RoCoF of Equation S1b scales linearly with H_{tot}, the average RoCoF that is commonly used as a protection signal often improves due to the fast response of AC-GFM CIG (8, 10). Moreover, in a CIG-dominated system, a large RoCoF is no longer indicative of a fault, and, in our opinion, its role as a protection signal should be reconsidered. Overall, virtual inertia is neither necessary nor a good fit for the VSC characteristics (see Section 2.3.2). Instead, future work should focus on fully leveraging the flexible and fast response of VSCs to overcome fundamental challenges that limit the integration of CIG into large-scale systems.

4.2. Converter-Interfaced Generation Interoperability and Integration Limits

While tremendous progress has been made on control and analysis of CIG across various spatial and temporal scales, the two closely related challenges of characterizing CIG interoperability and integration limits largely remain open. A key challenge is ensuring the interoperability of a large number of heterogeneous CIG devices (possibly using proprietary controls) and conventional

SGs through technology-agnostic specifications. The only well-understood cases are power systems that contain solely SGs or identical AC-GFM VSCs. For example, analytical results are available for a few specific CIG controls and dynamic circuit models (45–47). Moreover, a stability analysis framework for frequency dynamics of heterogeneous devices interconnected through quasi-steady-state network models has been developed (104). However, no analytic stability conditions are available that prevent adverse interactions of heterogeneous generation technologies across physics, control, and overlapping timescales. Therefore, interoperability across different technologies and timescales can, so far, only be studied numerically using high-fidelity simulations and models (5, 8, 105, 106) that may not be available in practice (due to, e.g., proprietary models). Studies along those lines often attempt to frame the problem in terms of a safe CIG integration percentage or the minimum share of AC-GFM CIG. However, depending on the system topology and controls in question, results can differ substantially, and numerous adverse interactions between physics and controls of VSCs and SGs as well as the grid dynamics have been identified (5, 8). We emphasize that the complexity significantly increases if the generation (e.g., wind turbines and solar photovoltaics) interfaced by the VSC is accounted for.

Overall, all of the aforementioned studies and results point to the need for stability conditions and analysis tools that are largely agnostic to the underlying technology and grid topology and can be used to ensure interoperability between different generation technologies and better understand fundamental CIG integration limits and system resilience.

5. SYSTEM-LEVEL SERVICES AND CONTROL

The previous sections have focused predominantly on the synchronization problem, i.e., how to massively integrate CIG in a power system so that the entire system robustly synchronizes. Whereas this task was previously naturally accomplished by the SG's physics, the synchronization of CIG must be enabled by means of control. Once the CIG has been synchronized, the next questions concern what it should actually contribute to the grid. Ideally, it should serve the same roles as rotational generation does nowadays: provide a (somewhat dispatchable) baseline power injection and grid support similar to SGs, namely, ancillary services supporting voltage and frequency on all timescales but also, in case of faults, short-circuit current and inertial response—both of which an SG provides by its physical design. This section discusses such system-level stability and control topics in low-inertia systems.

5.1. Dispatch and Allocation of Fast Frequency Response by Converter-Interfaced Generation

Section 4 introduced performance metrics concerning the power system frequency response, e.g., how nonrotational CIG may (or may not) lead to a larger nadir and steeper RoCoF of the COI frequency following a disturbance. The obvious remedy that has initially been advocated is to provide virtual inertia and/or damping through CIG. This insight is equally obvious and naive since low-inertia issues cannot be fixed by adding the inertia back to the system—partially for device-level reasons already discussed in the previous sections (e.g., see Sections 3.4.2 and 3.5), but there are also system-level aspects that warrant further scrutiny.

The initially prevalent folk theorem that adding more virtual inertia and damping makes a low-inertia system more robust has been disproved in many case studies, and nowadays the insight prevails that their careful tuning and spatial allocation over the network have a much more profound impact (for representative studies, see 62, 102, 107–110). A distilled summary of the conclusions is as follows. First, the well-planned spatial allocation of fast frequency response (i.e., virtual inertia and damping) has a much more profound impact than the total amount. Second, heuristic placements (e.g., uniformly across the grid) are rarely optimal, but the location of existing rotational generation as well as of faults (or their anticipated probability) needs to be taken into account. In simplified settings, the optimal allocation is actually collocated with the likelihood of local perturbations (107). Finally, the signal causality (i.e., GFL or GFM implementation) also has profound impacts: GFL implementations rely primarily on damping (due to a delay incurred by estimating $\frac{\mathrm{d}}{\mathrm{d}t}\omega$) and are often located near rotational generation, where the PLL-measured frequency is less fluctuating. By contrast, GFM CIG is more uniformly allocated.

Furthermore, the choice of cost function strongly affects the allocation of fast frequency response: Costs range from spectral criteria placing poles inside a predefined damping cone, over specifications on the post-disturbance response (see **Figure 8**), to system norms such as $\mathcal{H}_2$ and $\mathcal{H}_\infty$ (see 111). As is well known from the robust control literature, the system spectrum is often misleading when it comes to transient performance, and time-domain specifications are intractable. These considerations make system norms attractive formulations, particularly the computationally tractable $\mathcal{H}_2$ norm. In this regard, it turns out to be important not only to optimize performance but also to penalize control effort to obtain economic solutions.

The above insights on spatial allocation of fast frequency response have by now also led to considerations on the economic side, such as including the spatial allocation in a security-constrained generation dispatch or in virtual inertia markets (see 11, 12, 109, 112).

Finally, the system norm approach to quantify the effect of fast frequency response has spilled over from the system level to the device level. For example, multiple works have put forward fast frequency response designs for GFM and GFL converters based on $\mathcal{H}_2/\mathcal{H}_\infty$ approaches (e.g., 100, 101, 113–115), and the classification of CIG into forming and following devices based on system responses has been considered (65).

5.2. Ancillary Services Distributed Across Distributed Generation

Future power systems will contain an increasing penetration of nonrotational, renewable, and distributed energy resources. Hence, the reliable provision of ancillary services, as currently ensured by SGs, must be shouldered by distributed energy resources. This imposes great challenges to cope with intermittent renewables, as well as the device-specific limitations of CIG. A baseline solution is provided by ancillary service markets, where each participating unit must be able to provide ancillary services. However, individual units are often constrained in terms of power, energy, ramp rates, and so on. As a remedy, units are often pooled by aggregators to collectively bid on the market. This concept, known as a virtual power plant (116), has been applied to slow and static services such as providing a nominal power injection. Within the scope of this article, we focus on the refined concept of a dynamic virtual power plant (DVPP) able to provide dynamic (i.e., fast) ancillary services for low-inertia systems.

A DVPP is a collection of heterogeneous devices (complementing each other in terms of energy/power availability, ramp rates, and weather dependency) that must be coordinated to collectively provide reliable dynamic ancillary services across all energy/power levels and timescales, while none of the individual devices is able to do so by itself (117). Examples include hydropower with initially inverse response dynamics compensated by batteries on short timescales (118), synchronous condensers (with rotational energy) paired with converter-based generation (119), and hybrid storage pairing batteries with supercapacitors providing regulation on different frequency ranges (120). Custom solutions have been proposed for each of these cases, but an overarching control concept for DVPPs has been recently put forward (121–123), which is schematically illustrated in **Figure 9**.

To stay with the example from **Figure 9**, consider a set of generating units connected to the same bus of the high-voltage transmission grid. Consider a desired aggregate specification on the

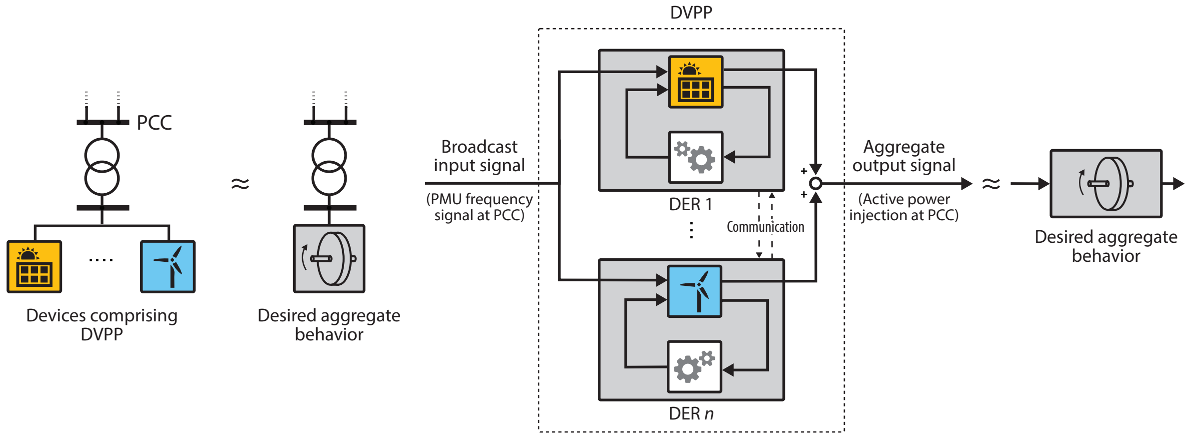

Figure 9

Schematic illustration of a DVPP. Here, different DERs are pooled so that their aggregate input–output behavior—defined as the mapping from the frequency to the power injection at the PCC—matches a desired specification, e.g., the response of a synchronous machine. Abbreviations: DER, distributed energy resource; DVPP, dynamic virtual power plant; PCC, point of common coupling; PMU, phasor measurement unit.

system level in the form of a dynamic response from a broadcast signal to an aggregate output, e.g., in a GFL fast frequency response setting a proportional–derivative (PD)–type transfer function (accounting for virtual damping and inertia) from a measured frequency signal to the aggregate power output of all devices. Given such an aggregate specification, the first step is to disaggregate it from the system level to individual devices, e.g., by broadcasting an error signal (121) to local controllers or customizing it device by device via dynamic participation factors (e.g., filtering depending on the devices' power levels and bandwidths) (122, 123). The second step is to match the disaggregated local device-level specifications subject to the device-level constraints, e.g., current limits in the case of a CIG device. Solutions range from mere tracking control to decentralized, optimal, and adaptive model matching control, accounting for intermittent device capacities and state constraints.

Multiple case studies have demonstrated that a DVPP approach brings tremendous improvements over noncoordinated local control actions, and it can match (and sometimes even outperform) the dynamic behavior by SGs. However, the setup in **Figure 9** is of limited scope and needs to be extended to the GFM and spatially distributed setting.

6. CONCLUSIONS AND OPEN PROBLEMS

In this survey, we reviewed modeling and control challenges of low-inertia power systems, at both the device and system level, and discussed solutions that have been put forward. Overall, we conclude that classical concepts for modeling, stability analysis, simulation, and control of power systems and classical concepts for control of power electronics need to be revisited in light of the transition to low-inertia and converter-dominated power systems. Here, we focused predominantly on novel aspects or traditional concepts that need to be revised in control of low-inertia power systems. Inevitably, this article does not present all viewpoints on and facets of the topic of low-inertia power systems. For instance, we barely scratched the surface of the important roles of markets and policies, energy storage technologies, variability of renewable generation, and demand response, to name a few. In all of these aspects, control and optimization play vital roles. It is our firm belief that the system-theoretic mindset is essential to bridge different communities and understand the complex interactions in a power system.

SUMMARY POINTS

1. Control and systems theory can serve as the lingua franca that translates specifications between power systems and power electronics.
2. The dynamics of synchronous generators and voltage source converters are structurally similar, but their limitations and the scales of the parameters are vastly different.
3. AC grid-forming converters can replace the fast inertia and slow turbine response of synchronous generators. From a control and systems point of view, there is no need for an artificial notion of virtual inertia as a means of fast frequency response.
4. Distributed energy resources need to be coordinated (e.g., in the form of virtual power plants) to fully leverage their potential to improve system-level performance.

FUTURE ISSUES

1. Analytical stability certificates need to be developed for converter-interfaced generation to overcome interoperability challenges and integration limits resulting from adverse interactions across spatial and temporal scales and heterogeneous technologies.
2. Advanced grid-forming control needs to explicitly account for the dynamics and constraints of renewable generation, energy storage, and power converters.
3. Grid-forming dynamic virtual power plants for spatially distributed and grid-forming distributed energy resources are required to fully leverage their potential.

DISCLOSURE STATEMENT

The authors are not aware of any affiliations, memberships, funding, or financial holdings that might be perceived as affecting the objectivity of this review.

ACKNOWLEDGMENTS

This article is based on work supported by the European Union's Horizon 2020 research and innovation program (Grant Agreement 883985) and work supported by the U.S. Department of Energy's Office of Energy Efficiency and Renewable Energy (EERE) under the Solar Energy Technologies Office Award Number 38637. The views expressed herein do not necessarily represent the views of the U.S. Department of Energy or the United States Government.

LITERATURE CITED

1. Milano F, Dörfler F, Hug G, Hill DJ, Verbič G. 2018. Foundations and challenges of low-inertia systems. In *2018 Power Systems Computation Conference*. Piscataway, NJ: IEEE. **https://doi.org/10.23919/PSCC.2018.8450880**
2. Fang J, Li H, Tang Y, Blaabjerg F. 2018. On the inertia of future more-electronics power systems. *IEEE Trans. Emerg. Sel. Top. Power Electron.* 7:2130–46
3. Winter W, Elkington K, Bareux G, Kostevc J. 2015. Pushing the limits: Europe's new grid: innovative tools to combat transmission bottlenecks and reduced inertia. *IEEE Power Energy Mag.* 13(1):60–74

4. Tielens P, Hertem DV. 2016. The relevance of inertia in power systems. *Renew. Sust. Energy Rev.* 55:999–1009
5. Markovic U, Stanojev O, Aristidou P, Vrettos E, Callaway D, Hug G. 2021. Understanding small-signal stability of low-inertia systems. *IEEE Trans. Power Syst.* 36:3997–4017
6. Taylor JA, Dhople SV, Callaway DS. 2016. Power systems without fuel. *Renew. Sust. Energy Rev.* 57:1322–36
7. Kroposki B, Johnson B, Zhang Y, Gevorgian V, Denholm P, et al. 2017. Achieving a 100% renewable grid: operating electric power systems with extremely high levels of variable renewable energy. *IEEE Power Energy Mag*. 15(2):61–73
8. Crivellaro A, Tayyebi A, Gavriluta C, Groß D, Anta A, et al. 2020. Beyond low-inertia systems: massive integration of grid-forming power converters in transmission grids. In *2020 IEEE Power and Energy Society General Meeting*. Piscataway, NJ: IEEE. **https://doi.org/10.1109/PESGM41954.2020.9282031**
9. Paolone M, Gaunt T, Guillaud X, Liserre M, Meliopoulos S, et al. 2020. Fundamentals of power systems modelling in the presence of converter-interfaced generation. *Electr. Power Syst. Res.* 189:106811
10. Tayyebi A, Groß D, Anta A, Kupzog F, Dörfler F. 2020. Frequency stability of synchronous machines and grid-forming power converters. *IEEE Trans. Emerg. Sel. Top. Power Electron.* 8:1004–18
11. Meegahapola L, Mancarella P, Flynn D, Moreno R. 2021. Power system stability in the transition to a low carbon grid: a techno-economic perspective on challenges and opportunities. *WIREs Energy Environ*. 10:e399
12. Mancarella P, Billimoria F. 2021. The fragile grid: the physics and economics of security services in low-carbon power systems. *IEEE Power Energy Mag*. 19(2):79–88
13. Dörfler F, Bolognani S, Simpson-Porco JW, Grammatico S. 2019. Distributed control and optimization for autonomous power grids. In *2019 18th European Control Conference*, pp. 2436–53. Piscataway, NJ: IEEE
14. Kundur P. 1994. *Power System Stability and Control*. New York: McGraw-Hill
15. Machowski J, Lubosny Z, Bialek JW, Bumby JR. 2020. *Power System Dynamics: Stability and Control*. Hoboken, NJ: Wiley & Sons
16. Yazdani A, Iravani R. 2010. *Voltage-Sourced Converters in Power Systems: Modeling, Control, and Applications*. Hoboken, NJ: Wiley & Sons
17. Schiffer J, Zonetti D, Ortega R, Stanković AM, Sezi T, Raisch J. 2016. A survey on modeling of microgrids—from fundamental physics to phasors and voltage sources. *Automatica* 74:135–50
18. Dörfler F, Simpson-Porco JW, Bullo F. 2018. Electrical networks and algebraic graph theory: models, properties, and applications. *Proc. IEEE* 106:977–1005
19. van der Schaft AJ, Stegink T. 2016. Perspectives in modeling for control of power networks. *Annu. Rev. Control* 41:119–32
20. Stevenson W, Grainger J. 1994. *Power System Analysis*. New York: McGraw-Hill Educ.
21. Kersting W. 2001. *Distribution System Modeling and Analysis*. Boca Raton, FL: CRC
22. Sauer PW, Pai MA, Chow JH. 2017. *Power System Dynamics and Stability: With Synchrophasor Measurement and Power System Toolbox*. Hoboken, NJ: Wiley & Sons
23. Akagi H, Watanabe EH, Aredes M. 2017. *Instantaneous Power Theory and Applications to Power Conditioning*. Hoboken, NJ: Wiley & Sons
24. Jeltsema D. 2015. Budeanu's concept of reactive and distortion power revisited. In *2015 International School on Nonsinusoidal Currents and Compensation*. Piscataway, NJ: IEEE. **https://doi.org/10.1109/ISNCC.2015.7174697**
25. O'Rourke CJ, Qasim MM, Overlin MR, Kirtley JL. 2019. A geometric interpretation of reference frames and transformations: dq0, Clarke, and Park. *IEEE Trans. Energy Convers.* 34:2070–83
26. Groß D, Arghir C, Dörfler F. 2018. On the steady-state behavior of a nonlinear power system model. *Automatica* 90:248–54
27. Chang HD, Chu CC, Cauley G. 1995. Direct stability analysis of electric power systems using energy functions: theory, applications, and perspective. *Proc. IEEE* 83:1497–529
28. Stegink TW, De Persis C, van der Schaft AJ. 2019. An energy-based analysis of reduced-order models of (networked) synchronous machines. *Math. Comput. Model. Dyn. Syst.* 25:1–39

29. Paganini F, Mallada E. 2020. Global analysis of synchronization performance for power systems: bridging the theory-practice gap. *IEEE Trans. Autom. Control* 65:3007–22
30. Venezian E, Weiss G. 2016. A warning about the use of reduced models of synchronous generators. In *2016 IEEE International Conference on the Science of Electrical Engineering*. Piscataway, NJ: IEEE. **https://doi.org/10.1109/ICSEE.2016.7806190**
31. Monshizadeh P, De Persis C, Monshizadeh N, van der Schaft AJ. 2016. Nonlinear analysis of an improved swing equation. In *2016 IEEE 55th Conference on Decision and Control*, pp. 4116–21. Piscataway, NJ: IEEE
32. Ajala O, Domínguez-Garcia A, Sauer P, Liberzon D. 2020. A library of second-order models for synchronous machines. *IEEE Trans. Power Syst.* 35:4803–14
33. Min H, Paganini F, Mallada E. 2019. Accurate reduced order models for coherent synchronous generators. In *2019 57th Annual Allerton Conference on Communication, Control, and Computing*, pp. 316–17. Piscataway, NJ: IEEE
34. Zhou D, Song Y, Blaabjerg F. 2018. Control of wind turbine system. In *Control of Power Electronic Converters and Systems*, ed. F Blaabjerg, pp. 269–98. London: Academic
35. Teodorescu R, Liserre M, Rodriguez P. 2011. *Grid Converters for Photovoltaic and Wind Power Systems*. Chichester, UK: Wiley & Sons
36. Hill DJ, Mareels IM. 1990. Stability theory for differential/algebraic systems with application to power systems. *IEEE Trans. Circuits Syst.* 37:1416–23
37. Hiskens IA, Hill DJ. 1989. Energy functions, transient stability and voltage behaviour in power systems with nonlinear loads. *IEEE Trans. Power Syst.* 4:1525–33
38. Dörfler F, Bullo F. 2012. Kron reduction of graphs with applications to electrical networks. *IEEE Trans. Circuits Syst. I* 60:150–63
39. Molzahn DK, Hiskens IA. 2019. *A Survey of Relaxations and Approximations of the Power Flow Equations*. Hanover, MA: Now
40. Misyris GS, Chatzivasileiadis S, Weckesser T. 2021. Grid-forming converters: sufficient conditions for RMS modeling. *Electr. Power Syst. Res.* 197:107324
41. Hatziargyriou N, Milanovic J, Rahmann C, Ajjarapu V, Canizares C, et al. 2020. Definition and classification of power system stability – revisited & extended. *IEEE Trans. Power Syst.* 36:3271–81
42. Vorobev P, Huang PH, Al Hosani M, Kirtley JL, Turitsyn K. 2017. High-fidelity model order reduction for microgrids stability assessment. *IEEE Trans. Power Syst.* 33:874–87
43. Raza M, Prieto-Araujo E, Gomis-Bellmunt O. 2017. Small-signal stability analysis of offshore AC network having multiple VSC-HVDC systems. *IEEE Trans. Power Deliv.* 33:830–39
44. Mariani V, Vasca F, Vasquez JC, Guerrero JM. 2014. Model order reductions for stability analysis of islanded microgrids with droop control. *IEEE Trans. Ind. Electron.* 62:4344–54
45. Vorobev P, Huang PH, Al Hosani M, Kirtley JL, Turitsyn K. 2017. A framework for development of universal rules for microgrids stability and control. In *2017 IEEE 56th Annual Conference on Decision and Control*, pp. 5125–30. Piscataway, NJ: IEEE
46. Subotić I, Groß D, Colombino M, Dörfler F. 2020. A Lyapunov framework for nested dynamical systems on multiple time scales with application to converter-based power systems. *IEEE Trans. Autom. Control* 66:5909–24
47. Groß D, Colombino M, Brouillon JS, Dörfler F. 2019. The effect of transmission-line dynamics on grid-forming dispatchable virtual oscillator control. *IEEE Trans. Control Netw. Syst.* 6:1148–60
48. Ortega R, van der Schaft AJ, Mareels I, Maschke B. 2001. Putting energy back in control. *IEEE Control Syst. Mag.* 21(2):18–33
49. Arghir C, Jouini T, Dörfler F. 2018. Grid-forming control for power converters based on matching of synchronous machines. *Automatica* 95:273–82
50. Arghir C, Dörfler F. 2019. The electronic realization of synchronous machines: model matching, angle tracking, and energy shaping techniques. *IEEE Trans. Power Electron.* 35:4398–410
51. Li C, Cvetkovic I, Burgos R, Boroyevich D. 2018. Assessment of virtual synchronous machine based control in grid-tied power converters. In *2018 International Power Electronics Conference*, pp. 790–94. Piscataway, NJ: IEEE

52. Huang L, Xin H, Wang Z, Wu K, Wang H, et al. 2017. A virtual synchronous control for voltage-source converters utilizing dynamics of DC-link capacitor to realize self-synchronization. *IEEE Trans. Emerg. Sel. Top. Power Electron.* 5:1565–77
53. Curi S, Groß D, Dörfler F. 2017. Control of low-inertia power grids: a model reduction approach. In *2017 IEEE 56th Annual Conference on Decision and Control*, pp. 5708–13. Piscataway, NJ: IEEE
54. Groß D, Sánchez-Sánchez E, Prieto-Araujo E, Gomis-Bellmunt O. 2022. Dual-port grid-forming control of MMCs and its applications to grids of grids. *IEEE Trans. Power Deliv*. 37:4721–35
55. Groß D, Dörfler F. 2017. On the steady-state behavior of low-inertia power systems. *IFAC-PapersOnLine* 50(1):10735–41
56. Rocabert J, Luna A, Blaabjerg F, Rodríguez P. 2012. Control of power converters in AC microgrids. *IEEE Trans. Power Electron.* 27:4734–49
57. Simpson-Porco JW, Dörfler F, Bullo F. 2017. Voltage stabilization in microgrids via quadratic droop control. *IEEE Trans. Autom. Control* 62:1239–53
58. Capitanescu F, Martinez Ramos J, Panciatici P, Kirschen D, Marano Marcolini A, et al. 2011. State-of-the-art, challenges, and future trends in security constrained optimal power flow. *Electr. Power Syst. Res.* 81:1731–41
59. Dörfler F, Chertkov M, Bullo F. 2013. Synchronization in complex oscillator networks and smart grids. *PNAS* 110:2005–10
60. Schiffer J, Ortega R, Astolfi A, Raisch J, Sezi T. 2014. Conditions for stability of droop-controlled inverter-based microgrids. *Automatica* 50:2457–69
61. Gomis-Bellmunt O, Sánchez-Sánchez E, Arévalo-Soler J, Prieto-Araujo E. 2021. Principles of operation of grids of DC and AC subgrids interconnected by power converters. *IEEE Trans. Power Deliv.* 36:1107–17
62. Poolla BK, Groß D, Dörfler F. 2019. Placement and implementation of grid-forming and grid-following virtual inertia and fast frequency response. *IEEE Trans. Power Syst.* 34:3035–46
63. Colombino M, Groß D, Brouillon JS, Dörfler F. 2019. Global phase and magnitude synchronization of coupled oscillators with application to the control of grid-forming power inverters. *IEEE Trans. Autom. Control* 64:4496–511
64. Lasseter RH, Chen Z, Pattabiraman D. 2020. Grid-forming inverters: a critical asset for the power grid. *IEEE Trans. Emerg. Sel. Top. Power Electron.* 8:925–35
65. Debry MS, Denis G, Prevost T. 2019. Characterization of the grid-forming function of a power source based on its external frequency smoothing capability. In *2019 IEEE Milan PowerTech*. Piscataway, NJ: IEEE. **https://doi.org/10.1109/PTC.2019.8810409**
66. Chung SK. 2000. A phase tracking system for three phase utility interface inverters. *IEEE Trans. Power Electron.* 15:431–38
67. Dong D, Wen B, Boroyevich D, Mattavelli P, Xue Y. 2015. Analysis of phase-locked loop low-frequency stability in three-phase grid-connected power converters considering impedance interactions. *IEEE Trans. Ind. Electron.* 62:310–21
68. Jafarpour S, Purba V, Johnson B, Dhople S, Bullo F. 2021. Singular perturbation and small-signal stability for inverter networks. *IEEE Trans. Control Netw. Syst.* 9:979–92
69. Bevrani H, Ise T, Miura Y. 2014. Virtual synchronous generators: a survey and new perspectives. *Int. J. Electr. Power Energy Syst.* 54:244–54
70. Bala S, Venkataramanan G. 2010. On the choice of voltage regulators for droop-controlled voltage source converters in microgrids to ensure stability. In *2010 IEEE Energy Conversion Congress and Exposition*, pp. 3448–55. Piscataway, NJ: IEEE
71. Cvetkovic I, Boroyevich D, Burgos R, Li C, Mattavelli P. 2015. Modeling and control of grid-connected voltage-source converters emulating isotropic and anisotropic synchronous machines. In *2015 IEEE 16th Workshop on Control and Modeling for Power Electronics*. Piscataway, NJ: IEEE. **https://doi.org/10.1109/COMPEL.2015.7236454**
72. Pogaku N, Prodanovic M, Green TC. 2007. Modeling, analysis and testing of autonomous operation of an inverter-based microgrid. *IEEE Trans. Power Electron.* 22:613–25
73. D'Arco S, Suul JA, Fosso AB. 2015. A Virtual Synchronous Machine implementation for distributed control of power converters in SmartGrids. *Electr. Power Syst. Res.* 122:180–97

74. Ajala O, Lu M, Dhople S, Johnson BB, Dominguez-Garcia A. 2021. Model reduction for inverters with current limiting and dispatchable virtual oscillator control. *IEEE Trans. Energy Convers*. 37:2250–59
75. Qoria T, Gruson F, Colas F, Guillaud X, Debry MS, Prevost T. 2018. Tuning of cascaded controllers for robust grid-forming voltage source converter. In *2018 Power Systems Computation Conference*. Piscataway, NJ: IEEE. **https://doi.org/10.23919/PSCC.2018.8443018**
76. Johnson B, Salapaka S, Lundstrom B, Salapaka M. 2016. Optimal structures for voltage controllers in inverters. In *22nd International Symposium on Mathematical Theory of Networks and Systems*, pp. 596–601. Minneapolis: Univ. Minn.
77. Paquette AD, Divan DM. 2015. Virtual impedance current limiting for inverters in microgrids with synchronous generators. *IEEE Trans. Ind. Appl.* 51:1630–38
78. Xin H, Huang L, Zhang L, Wang Z, Hu J. 2016. Synchronous instability mechanism of $p-f$ droop-controlled voltage source converter caused by current saturation. *IEEE Trans. Power Syst.* 31:5206–7
79. He J, Li YW. 2011. Analysis, design, and implementation of virtual impedance for power electronics interfaced distributed generation. *IEEE Trans. Ind. Appl.* 47:2525–38
80. Groß D, Dörfler F. 2019. Projected grid-forming control for current-limiting of power converters. In *2019 57th Annual Allerton Conference on Communication, Control, and Computing*, pp. 326–33. Piscataway, NJ: IEEE
81. Chandorkar M, Divan D, Adapa R. 1993. Control of parallel connected inverters in standalone AC supply systems. *IEEE Trans. Ind. Appl.* 29:136–43
82. Zhang L, Harnefors L, Nee HP. 2010. Power-synchronization control of grid-connected voltage-source converters. *IEEE Trans. Power Syst.* 25:809–20
83. Zhong QC, Weiss G. 2011. Synchronverters: inverters that mimic synchronous generators. *IEEE Trans. Ind. Electron.* 58:1259–67
84. Schiffer J, Goldin D, Raisch J, Sezi T. 2013. Synchronization of droop-controlled microgrids with distributed rotational and electronic generation. In *52nd IEEE Conference on Decision and Control*, pp. 2334–39. Piscataway, NJ: IEEE
85. D'Arco S, Suul JA. 2013. Virtual synchronous machines – classification of implementations and analysis of equivalence to droop controllers for microgrids. In *2013 IEEE Grenoble PowerTech*. Piscataway, NJ: IEEE. **https://doi.org/10.1109/PTC.2013.6652456**
86. D'Arco S, Suul JA. 2014. Equivalence of virtual synchronous machines and frequency-droops for converter-based microgrids. *IEEE Trans. Smart Grid* 5:394–95
87. Fouad A, Vittal V. 1988. The transient energy function method. *Int. J. Electr. Power Energy Syst.* 10:233–46
88. Chiang HD. 2011. *Direct Methods for Stability Analysis of Electric Power Systems: Theoretical Foundation, BCU Methodologies, and Applications*. Hoboken, NJ: Wiley & Sons
89. Gholami A, Sun A. 2021. Stability of multi-microgrids: new certificates, distributed control, and Braess's paradox. *IEEE Trans. Control Netw. Syst.* 9:308–19
90. Aracil J, Gordillo F. 2002. On the control of oscillations in DC-AC converters. In *IEEE 2002 28th Annual Conference of the Industrial Electronics Society*, Vol. 4, pp. 2820–25. Piscataway, NJ: IEEE
91. Tôrres LAB, Hespanha JP, Moehlis J. 2012. Power supply synchronization without communication. In *2012 IEEE Power and Energy Society General Meeting*. Piscataway, NJ: IEEE. **https://doi.org/10.1109/PESGM.2012.6344905**
92. Johnson BB, Dhople SV, Hamadeh AO, Krein PT. 2014. Synchronization of parallel single-phase inverters with virtual oscillator control. *IEEE Trans. Power Electron.* 29:6124–38
93. Tôrres LAB, Hespanha JP, Moehlis J. 2015. Synchronization of identical oscillators coupled through a symmetric network with dynamics: a constructive approach with applications to parallel operation of inverters. *IEEE Trans. Autom. Control* 60:3226–41
94. Johnson BB, Sinha M, Ainsworth NG, Dörfler F, Dhople SV. 2016. Synthesizing virtual oscillators to control islanded inverters. *IEEE Trans. Power Electron.* 31:6002–15
95. Sinha M, Dörfler F, Johnson BB, Dhople SV. 2017. Uncovering droop control laws embedded within the nonlinear dynamics of Van der Pol oscillators. *IEEE Trans. Control Netw. Syst.* 4:347–58
96. Seo GS, Colombino M, Subotić I, Johnson B, Groß D, Dörfler F. 2019. Dispatchable virtual oscillator control for decentralized inverter-dominated power systems: analysis and experiments. In *2019 IEEE Applied Power Electronics Conference and Exposition*, pp. 561–66. Piscataway, NJ: IEEE

97. Awal MA, Husain I. 2021. Unified virtual oscillator control for grid-forming and grid-following converters. *IEEE Trans. Emerg. Sel. Top. Power Electron.* 9:4573–86
98. Subotić I, Groß D. 2022. Power-balancing dual-port grid-forming power converter control for renewable integration and hybrid AC/DC power systems. *IEEE Trans. Control Netw. Syst.* 9:1949–61
99. NERC (N. Am. Electr. Reliab. Corp.). 2017. *1,200 MW fault induced solar photovoltaic resource interruption disturbance report*. Rep., NERC, Atlanta, GA
100. Chen M, Zhou D, Tayyebi A, Prieto-Araujo E, Dörfler F, Blaabjerg F. 2022. Generalized multivariable grid-forming control design for power converters. *IEEE Trans. Smart Grid* 13:2873–85
101. Huang L, Xin H, Dörfler F. 2020. H_∞-control of grid-connected converters: design, objectives and decentralized stability certificates. *IEEE Trans. Smart Grid* 11:3805–16
102. Borsche TS, Liu T, Hill DJ. 2015. Effects of rotational inertia on power system damping and frequency transients. In *2015 54th IEEE Conference on Decision and Control*, pp. 5940–46. Piscataway, NJ: IEEE
103. Winkelman JR, Chow JH, Bowler BC, Avramovic B, Kokotovic PV. 1981. An analysis of interarea dynamics of multi-machine systems. *IEEE Trans. Power Appar. Syst.* PAS-100:754–63
104. Pates R, Mallada E. 2019. Robust scale-free synthesis for frequency control in power systems. *IEEE Trans. Control Netw. Syst.* 6:1174–84
105. Hoke A, Gevorgian V, Shah S, Koralewicz P, Kenyon RW, Kroposki B. 2021. Island power systems with high levels of inverter-based resources: stability and reliability challenges. *IEEE Electrif. Mag.* 9(1):74–91
106. Kenyon RW, Wang B, Hoke A, Tan J, Antonio C, Hodge BM. 2021. Validation of Maui PSCAD model: motivation, methodology, and lessons learned. In *2020 52nd North American Power Symposium*. Piscataway, NJ: IEEE. **https://doi.org/10.1109/NAPS50074.2021.9449773**
107. Poolla BK, Bolognani S, Dörfler F. 2017. Optimal placement of virtual inertia in power grids. *IEEE Trans. Autom. Control* 62:6209–20
108. Pulgar-Painemal H, Wang Y, Silva-Saravia H. 2017. On inertia distribution, inter-area oscillations and location of electronically-interfaced resources. *IEEE Trans. Power Syst.* 33:995–1003
109. Guggilam SS, Zhao C, Dall'Anese E, Chen YC, Dhople SV. 2018. Optimizing DER participation in inertial and primary-frequency response. *IEEE Trans. Power Syst.* 33:5194–205
110. Venkatraman A, Markovic U, Shchetinin D, Vrettos E, Aristidou P, Hug G. 2021. Improving dynamic performance of low-inertia systems through eigensensitivity optimization. *IEEE Trans. Power Syst.* 36:4075–88
111. Poolla BK, Groß D, Borsche T, Bolognani S, Dörfler F. 2018. Virtual inertia placement in electric power grids. In *Energy Markets and Responsive Grids*, ed. S Meyn, T Samad, I Hiskens, J Stoustrup, pp. 281–305. New York: Springer
112. Poolla BK, Bolognani S, Li N, Dörfler F. 2020. A market mechanism for virtual inertia. *IEEE Trans. Smart Grid* 11:3570–79
113. Jiang Y, Pates R, Mallada E. 2020. Dynamic droop control in low-inertia power systems. *IEEE Trans. Autom. Control* 66:3518–33
114. Tavakoli SD, Fekriasl S, Prieto-Araujo E, Beerten J, Gomis-Bellmunt O. 2021. Optimal H_∞ control design for MMC-based HVDC links. *IEEE Trans. Power Deliv.* 37:786–97
115. Sánchez-Sánchez E, Groß D, Prieto-Araujo E, Dörfler F, Gomis-Bellmunt O. 2019. Optimal multivariable MMC energy-based control for DC voltage regulation in HVDC applications. *IEEE Trans. Power Deliv.* 35:999–1009
116. Pudjianto D, Ramsay C, Strbac G. 2007. Virtual power plant and system integration of distributed energy resources. *IET Renew. Power Gener.* 1:10–16
117. Marinescu B, Gomis-Bellmunt O, Dörfler F, Schulte H, Sigrist L. 2021. Dynamic virtual power plant: a new concept for grid integration of renewable energy sources. arXiv:2108.00153 [eess.SY]
118. Ghasemi H, Melki J. 2019. *Investigation of frequency containment reserves with inertial response and batteries*. MS Thesis, KTH R. Inst. Technol., Stockholm
119. Kenyon RW, Hoke AF, Tan J, Kroposki BD, Hodge BS. 2020. *Grid-following inverters and synchronous condensers: a grid-forming pair?* Rep., Natl. Renew. Energy Lab., Golden, CO
120. Li W, Joos G. 2008. A power electronic interface for a battery supercapacitor hybrid energy storage system for wind applications. In *2008 IEEE Power Electronics Specialists Conference*, pp. 1762–68. Piscataway, NJ: IEEE

121. Zhong W, Chen J, Liu M, Murad MAA, Milano F. 2021. Coordinated control of virtual power plants to improve power system short-term dynamics. *Energies* 14:1182
122. Björk J, Johansson KH, Dörfler F. 2022. Dynamic virtual power plant design for fast frequency reserves: coordinating hydro and wind. *IEEE Trans. Control Netw. Syst.* In press. **https://doi.org/10.1109/TCNS.2022.3181553**
123. Haberle V, Fisher MW, Araujo EP, Dörfler F. 2021. Control design of dynamic virtual power plants: an adaptive divide-and-conquer approach. *IEEE Trans. Power Syst.* 37:4040–55